Hindawi Publishing Corporation
Journal of Nanomaterials
Volume 2015, Article ID 854094, 20 pages
http://dx.doi.org/10.1155/2015/854094

Review Article

Recent Progress in Ohmic/Schottky-Contacted ZnO Nanowire Sensors

Xiaoli Zhao,[1] Ranran Zhou,[1] Qilin Hua,[1] Lin Dong,[2] Ruomeng Yu,[3] and Caofeng Pan[1]

[1] *Beijing Institute of Nanoenergy and Nanosystems, Chinese Academy of Sciences, Beijing 100083, China*
[2] *School of Materials Science and Engineering, Zhengzhou University, Zhengzhou 450001, China*
[3] *School of Materials Science and Engineering, Georgia Institute of Technology, Atlanta, GA 30332-0245, USA*

Correspondence should be addressed to Lin Dong; ldong@zzu.edu.cn, Ruomeng Yu; ruomengyu@gatech.edu, and Caofeng Pan; cfpan@binn.cas.cn

Received 31 March 2015; Accepted 16 June 2015

Academic Editor: Meiyong Liao

We review the recent progress of zinc oxide (ZnO) nanowire sensors with ohmic-contacted and Schottky-contacted configurations and the enhancement of the performances of Schottky-contacted ZnO NW sensors (SCZNSs) by the piezotronic effect. Comparing with the traditional ohmic-contacted ZnO NW sensors (OCZNSs), the SCZNSs have higher sensitivities and faster responses controlled by the barrier height at the metal-semiconductor (M-S) interface. The piezotronic effect was applied to tune the Schottky barrier height (SBH) with the strain-induced piezoelectric polarization charges at the interface of the M-S contact. The piezotronic effect can thus improve the detection limitation, sensitivity, and response time of the SCZNSs in different applications, such as UV detection, gas and bio/chemical sensing. These piezotronic-enhanced SCZNSs may find potential applications in human-machine interfacing and flexible electronics skin technologies.

1. Introduction

One-dimensional semiconductor nanomaterials have been studied extensively and regarded as one of the most promising candidates for realizing ultrasensitive sensors because of their large surface-to-volume ratios, polarized crystal orientation, short distances for minority carriers to travel, and high carrier mobility [1–3]. Zinc oxide (ZnO), a direct wide band gap semiconductor material with wurtzite structure, has been widely studied due to its extraordinary electrical, optical, and piezoelectric properties [4–6]. ZnO nanowire (NW) with desired morphology and aspect ratio can be easily obtained through various methods such as vapor-liquid-solid (VLS) or vapor-solid (VS) process, wet chemical growth, molecular beam epitaxy (MBE), and metal-organic chemical vapor deposition (MOCVD) and has attracted particular interest in UV detection, gas and bio/chemical sensing areas [7–10].

Most ZnO NW sensors are composed of a single ZnO NW with two ends fixed by the metal electrodes. The contacts between the metals and the ZnO NWs can be either ohmic or Schottky. Generally, most NW sensors based on ohmic-contact are fabricated as field effect transistor (FET) structure, of which the current is controlled by modulating the "gate voltage" through the external adsorbed species. Although devices built with a NW of smaller diameter are expected to have improved detection limit and response time to the external stimuli because of its large surface-to-volume ratio, the fabrication process of devices with reduced dimension would be much more complicated and costly [11–16]. In order to further improve the sensitivity of the ohmic-contacted ZnO NW sensors (OCZNSs), some complicated methods have been applied, such as surface modification and post-anneal. Thus, the OCZNSs with smaller sized NW and higher specific surface make the device fabrication more complicated. In comparison, the performance of the Schottky-contacted ZnO NW sensors (SCZNSs) can be optimized by regulating the Schottky barrier height (SBH) at local metal-semiconductor (M-S) interface [17–19]. Therefore, higher sensitivity, faster response, and easier fabrication process can be achieved by SCZNS that consists of microwires with the diameter in the submicrometer range, and it

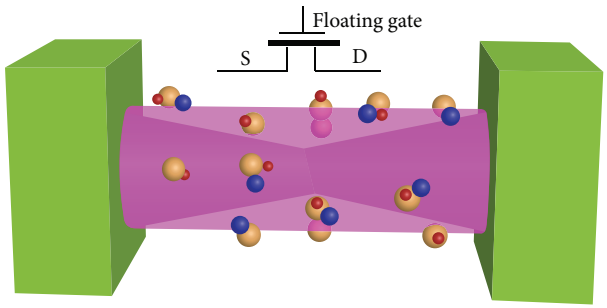

Figure 1: Schematic diagram of the working principle of a nanowire based nanosensor for a conventional FET configuration [3]. Copyright 2010, John Wiley and Sons.

aroused much interest in UV, gas and bio/chemical sensing system [20–24]. Wang's group introduced the piezotronic effect [25–28] to modulate the charge carriers generation, transport, and recombination process by tuning the SBH at the local M-S interface with strain-induced piezoelectric polarization charges, hence improving the performance of the SCZNSs.

Herein, this paper reviews recent research progresses in the OCZNSs and SCZNSs for UV, gas and bio/chemical sensing. The working principle and performance optimizations of the OCZNSs and the SCZNSs are explored. A wide range of SCZNS with enhanced performance tuned by the piezotronic effect is included in this paper.

2. Ohmic-Contacted ZnO NW Sensors (OCZNSs)

2.1. Working Principle of the OCZNS. Ohmic contacts formed between the metal electrodes and semiconducting nanomaterials are in a dominant position during the early ages [29, 30]. The most typical structure of the OCZNS is FET, which utilizes a ZnO NW as the essential building block, with both ends bonded to a rigid substrate [31, 32]. The mechanism of FET is that the voltage applied across the gate and source terminals controls the flow of charge carriers from the source to drain by affecting the size and distribution of a "conductive channel" [33, 34].

The amount of target molecules adsorbed on the surface of the ZnO NW can be deduced by the change of the conductance, because the adsorbed molecules may modify the surface charges and states, change the local work function and band alignment, and alter the gate potential and the carrier mobility [35–37]. These changes are defined as a floating gate effect on the conducting channel of the FET [38], as shown in Figure 1. In order to maximize the gate effect, thin and usually short NWs are chosen to fabricate the device to obtain a higher sensitivity.

2.2. UV-OCZNSs. ZnO is a very good candidate for photonic devices in the UV range, with a direct band gap of 3.4 eV and a large exciton binding energy of 60 meV at room temperature. Soci et al. [39] demonstrated a kind of visible blind UV-OCZNS with high internal gain. Under the UV illumination ($\lambda = 390$ nm, $P = 10\,\mu$W/cm^2), a time-resolved measurement over a broad temporal domain in different ambient conditions is conducted to measure the photoconductivity of the ZnO NW. The current in the ZnO NW increases by several orders of magnitude, and the photoconductive gain can reach a high value of $G \sim 10^8$. The presence of oxygen-related hole-trap states at the NW surface, which hinders the charge carrier recombination, is regarded as the major reason for such an extremely high internal gain.

Kim and Chu [40] investigated the bias and gate voltage effects on the UV-OCZNS. The sensitivity can be increased by tuning the drain-source voltage (V_{ds}) and gate-source voltage (V_{gs}), as shown in Figure 2. When the bias voltage V_{ds} increases from 1 mV to 1 V, the on/off ratio under a hand-held UV lamp ($\lambda = 365$ nm and $P = 0.47$ mW/cm^2) increases abruptly from ~70 to ~3×10^5, and the photocurrent increases from ~1 nA to ~1 μA. So at the optimal gate voltage ($V_{gs} = -1$ V) and bias voltage ($V_{ds} = 1$ V), the on/off ratio reaches its maximum value of ~10^6.

2.3. Gas-OCZNSs. ZnO NW has also been regarded as a promising candidate for gas sensing owing to its high electron mobility and good thermal stability under various gas conditions. Besides, ZnO can be adopted in a broad range of gases, both the oxidizing gas (O_2, NO) and the reducing gas (CO, H_2, H_2S).

Fan et al. [32] fabricated the O_2-OCZNS based on a single ZnO NW. The oxygen detection sensitivity can be modulated by the gate voltage. The ambient oxygen partial pressure has a considerable effect on the performance of the O_2-OCZNS, due to the conductivity changes caused by surface band bending, which is induced by O_2 molecule absorption. The corresponding current decreases when the oxygen pressure increases. The relevant conductance ($\Delta G/G_0$) decreases as the NW radius increases (Figure 3); thus, a smaller diameter ZnO NW exhibits a higher sensitivity. The maximum sensitivity of 64% appears at −1.4 V, which is above the gate threshold voltage (−2.0 V) in 10 ppm O_2.

The gas detection performance can be further enhanced by nanoparticles decoration. Joshi et al. [41] used Au decorated ZnO NWs to detect an invisible and odorless toxic gas, carbon monoxide (CO), at the room temperature. The Au nanoparticles are decorated on the ZnO NWs and act as a catalyst in chemical sensitization. A response time value of ~5 s is observed for 1000 ppm of CO in air. The improvement in gas sensing behavior is attributed to the transfer of electrons resulting from gas oxidation at the ZnO NWs surface.

2.4. Bio/Chemical-OCZNSs. ZnO NWs are widely adopted for bio/chemical sensors due to the advantages of ultralow detection limit, fast response, and impressive biocompatibility [42–45]. Liu et al. [46] synthesized a single ZnO NW-based biologically sensitive sensor for detection of different concentrations of uric acid solution. Before detecting, the surface of the ZnO NW is treated with the covalent modification method. The addition of uric acid with the concentrations from 1 pM to 0.5 mM resulted in the electrical conductance changes of up to 227 nS, and the response time turns out to be in the order of millisecond. The detection limit of the

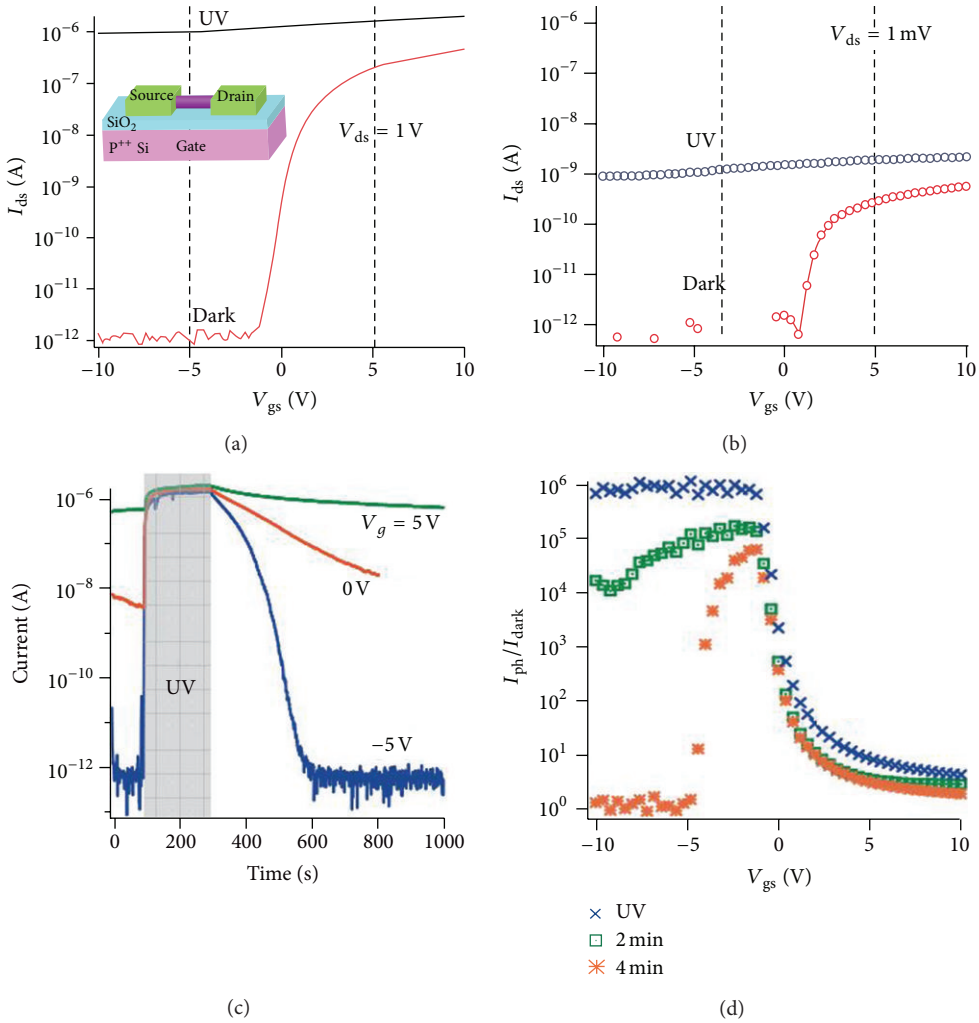

FIGURE 2: (a) Insert is a schematic of a ZnO NW FET. I_{ds}-V_{gs} characteristics under UV illumination and under darkness when $V_{ds} = 1$ V, and (b) when $V_{ds} = 1$ mV. (c) Drain-source current measured as a function of time ($I_{ds} - t$) while the light was on and off when $V_g = 5$ V, 0 V, and −5 V ($V_{ds} = 1$ V). (d) I_{ph}/I_{dark} as a function of gate voltage. Maximum I_{ph}/I_{dark} was obtained at $V_{gs} \sim -1$ V [40]. Copyright 2009, John Wiley and Sons.

ZnO NW biosensor can be as low as 1 pM with 14.7 nS of conductance increase.

Besides the detection of various biological molecules, the ZnO NW is also used as a pH sensor, ranging from 5 to 8.5 reported by Menzel et al. [47] after surface passivation of the ZnO NWs with a thin film of C_4F_8. The sensitivity of the pH-OCZNS obtained from the slope of the conductance reached -2.063 ± 0.14 (μS/pH). The conductance of ZnO NW exhibits linear response over a wide pH range instantly, which mainly stems from the change of the surface charge during the protonation and deprotonation.

A control experiment is conducted by investigating ZnO nanotubes (NTs) and nanorods (NRs) based pH sensors, elaborated by Fulati et al. [48]. Both pH sensors show a linear response to the pH values (Figure 4). The developed ZnO NTs electrochemical potential pH sensors show faster response and higher sensitivity than the ZnO NRs pH sensors with the same dimensions, due to more subsurface O_2 vacancies and adsorption sites exist in the ZnO NTs.

In summary, OCZNSs with one-dimensional nanostructure have high surface-to-volume ratio, which is a key point to enhance the sensitivity and response time of the device [35, 36, 49–52]. In addition, various methods have been explored to improve the sensitivity of the OCZNSs, such as choosing proper bias and gate voltage [32, 40], surface modification [41, 46, 47], and increasing the O_2 vacancies and adsorption sites [48]. However, sophisticated decoration and fabrication process of the nanostructures may prohibit the widespread applications of the OCZNSs.

3. Schottky-Contacted ZnO NW Sensors (SCZNSs)

Many researchers investigate the Schottky-contacted structure for fabricating high performance ZnO NW sensors, because the SCZNSs have a higher sensitivity, a faster-response sensing behavior, and a lower-cost fabrication process [39, 53–56].

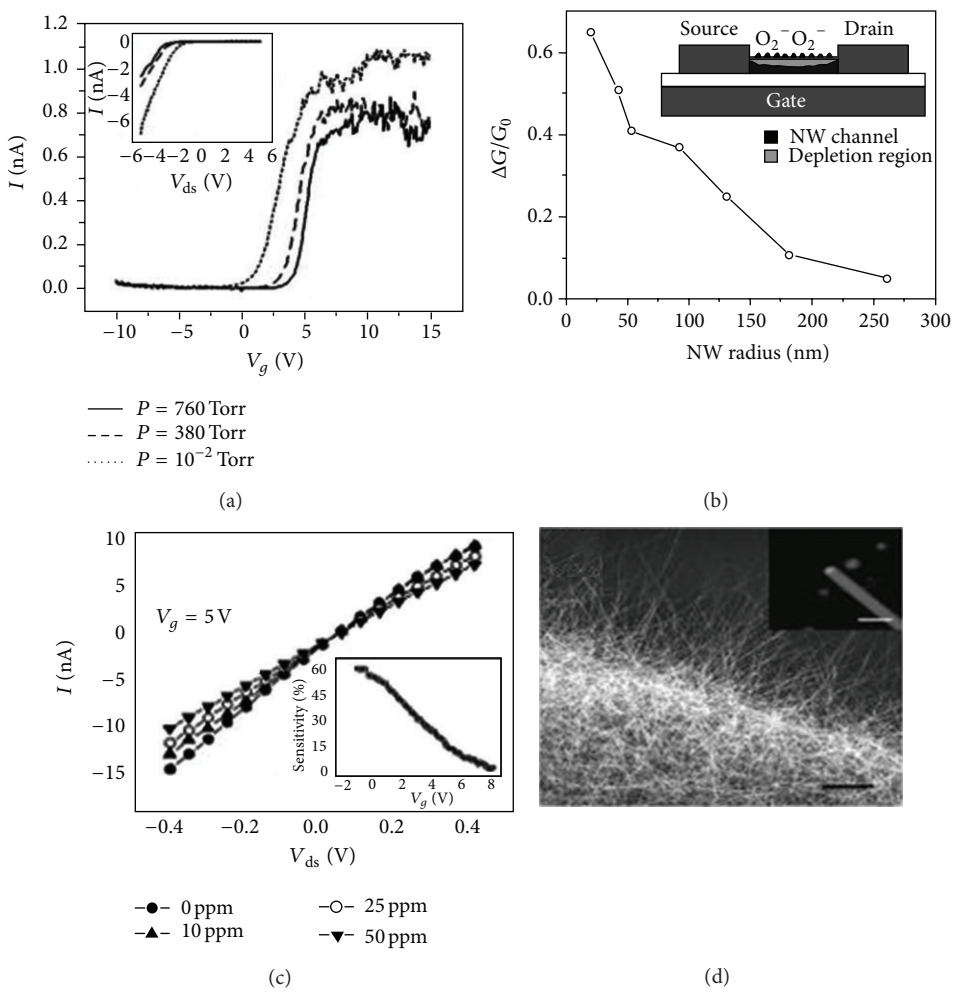

Figure 3: (a) Transconductance of a ZnO NW FET under different pressures at room temperature, and V_{ds} = 200 mV. Inset: I-V_{ds} curve of the NW under 760, 380, and 10^{-2} Torr. (b) Ratio of conductance change versus radius under a vacuum and atmosphere. Inset: a schematic of NW FET channel depletion (depicted by gray shading) caused by adsorption of oxygen molecules. (c) I-V_{ds} curves obtained in 0, 10, 25, and 50 ppm O_2 at V_g = 5 V. Conductance of ZnO NW decreases monotonically with increasing O_2 concentration. Inset: relationship between sensitivity and gate voltage. (d) FE-SEM image of as-grown ZnO NWs, scale bar is 20 μm. Inset image shows a single ZnO NW terminated with a gold nanoparticle, and scale bar is 100 nm [32]. Copyright 2004, AIP Publishing LLC.

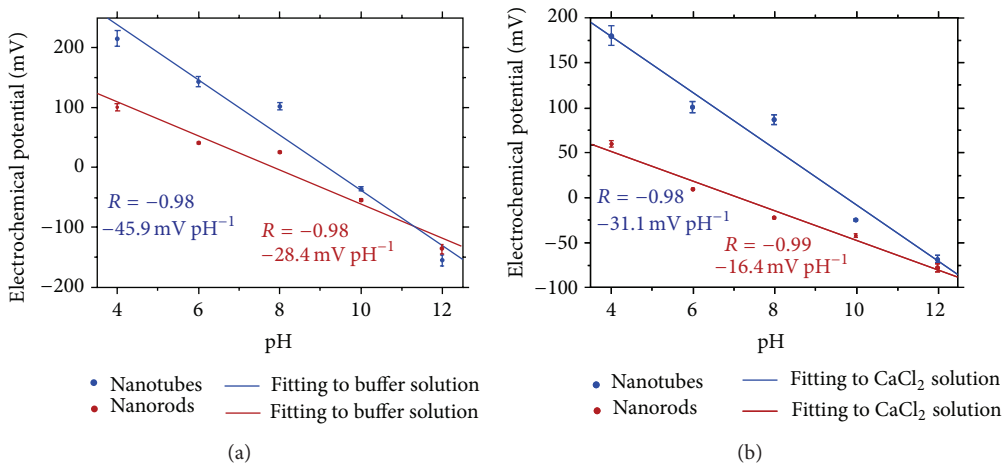

Figure 4: Experimental measurements of electrochemical potential versus pH comparison curves for ZnO nanorods and nanotubes immersed in (a) buffer and (b) $CaCl_2$ solutions [48]. Copyright 2009, Sensors.

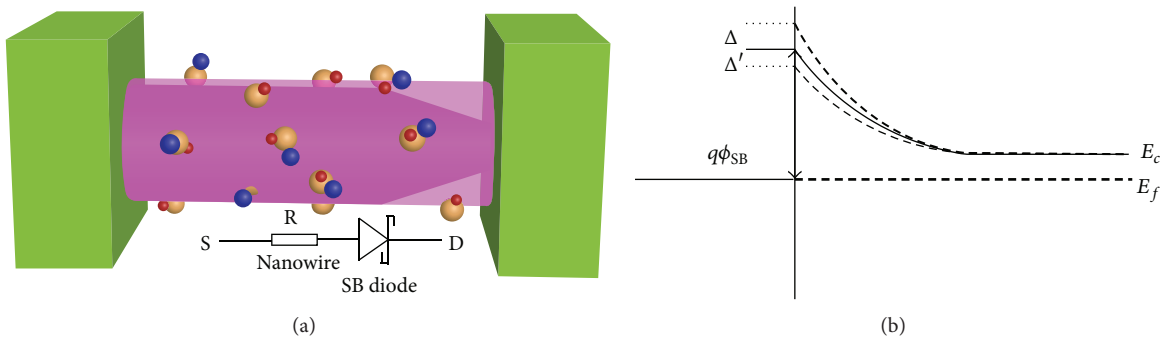

Figure 5: Schematic diagram of the working principle of a nanowire based nanosensor for (a) the Schottky-gated structure. (b) The energy-band diagram at the interface of the metal-ZnO contact, where a Schottky barrier is formed. The barrier height and width can be tuned in response to the change in the surrounding environment around the contact area [3]. Copyright 2010, John Wiley and Sons.

3.1. Working Principle of the SCZNSs. The typical SCZNSs contain Schottky barrier (SB) at least at one M-S interface, and the whole structure of the SCZNSs can be regarded as a NW with a SB diode in series (Figure 5). Therefore, the carrier transport through the whole device is dominated by the barrier height at local M-S interface [57], and the sensitivity is enhanced by changing the SBH at local M-S interface instead of the bulk conductance in the OCZNSs [58, 59].

The SBH at the local M-S interface plays a very important role in changing the carrier transport process. The original barrier height of local Schottky-contact is essential to the performance of the sensors, because an appropriate original barrier height of local Schottky-contact can promote the sensing performance. In order to further enhance the performance of the sensor, Wang presented the piezotronic effect [23, 60], which can change the original barrier height by inducing piezoelectric polarization charges at the local M-S interface. Therefore, the optimal performance of the Schottky-contacted sensor can be obtained.

3.2. Fundamentals of the Piezotronic Effect Enhanced the SCZNSs. Once the ZnO NW device is under strain, two typical effects may affect the carrier transport process. One is the piezoresistance effect, which is a common feature of any semiconductors, and this effect can change the band gap, charge carrier density, and possibly density of states in the conduction band of the semiconductor crystal under strain. The piezoresistance effect is a symmetric effect on the two end contacts and has no polarity, which will not affect the electrical performance of a sensor [61]. The other is the piezotronic effect [60, 62], a coupling effect between the semiconducting and piezoelectric properties of materials with non-Centro symmetric structure, such as the wurtzite and zinc blende family. ZnO has a hexagonal structure with a large anisotropic property in *c*-axis direction (Figure 6). The Zn^{2+} cations and O^{2-} anions are tetrahedrally coordinated, and the centers of the positive ions and negative ions overlap with each other in the strain-free condition. If a stress is applied at an apex of the tetrahedron, a dipole moment is generated since the centers of the cations and anions separated. The cumulative effect of the dipole moments by all tetrahedron units in the crystal results in a macroscopic potential diversification along the straining direction, that is, the piezoelectric potential (piezopotential).

For an n-type semiconductor and a metal contact, if the electron affinity of the semiconductor is lower than the work function of the metal, a SB is created at the interface. By applying a compressive or tensile strain from the external environment, a piezopotential distribution is induced in the semiconductor and piezoelectric polarization charges appear at the M-S interface in the semiconductor side, and they can affect the SBH at the M-S interface. Once a strain is created in the piezoelectric semiconductor, a negative piezopotential at the semiconductor side effectively increases the local SBH, while a positive piezopotential reduces the SBH [13, 30, 35, 43, 63–66]. As a result, for the Schottky-contacted sensors fabricated with the piezotronic semiconductor materials, external strains can be used as a "strain gate" to control the SBH and the electronic transport properties by inducing piezoelectric polarization charges at the local M-S interface. Thus, piezotronic effect can be used to optimize the performances of the SCZNSs.

3.3. UV-SCZNSs

3.3.1. UV-Sensors. Recently, based on the photoelectric property of individual ZnO NW, several important researches on the UV-SCZNSs have been published. Zhou et al. [59] grew the ZnO NWs by a VS process and transferred a single ZnO NW onto SiO_2/Si substrate, and Ti/Au and Pt electrodes were deposited at the end of the ZnO NW to obtain ohmic and Schottky-contact, respectively. They compared the response time of the UV-SCZNSs and the UV-OCZNSs. The ohmic structure and the characteristic of the OCZNSs are shown in Figure 7. Under the illumination of UV light ($\lambda = 365\,\text{nm}$, $P = 30\,\mu\text{W/cm}^2$), the photocurrent is still unsaturated in the OCZNSs after about 260 s and the recovery time is over 2500 s, whereas for the SCZNSs the current changes from 0.04 to 60 nA within 0.6 s, and the reset time is 0.8 s. The Schottky junction could dramatically enhance the sensitivity and improve the response/recovery time. The local electric field at the SB area quickly separates the electrons and holes generated by photon excitation, which increase the carrier lifetime and free carrier density.

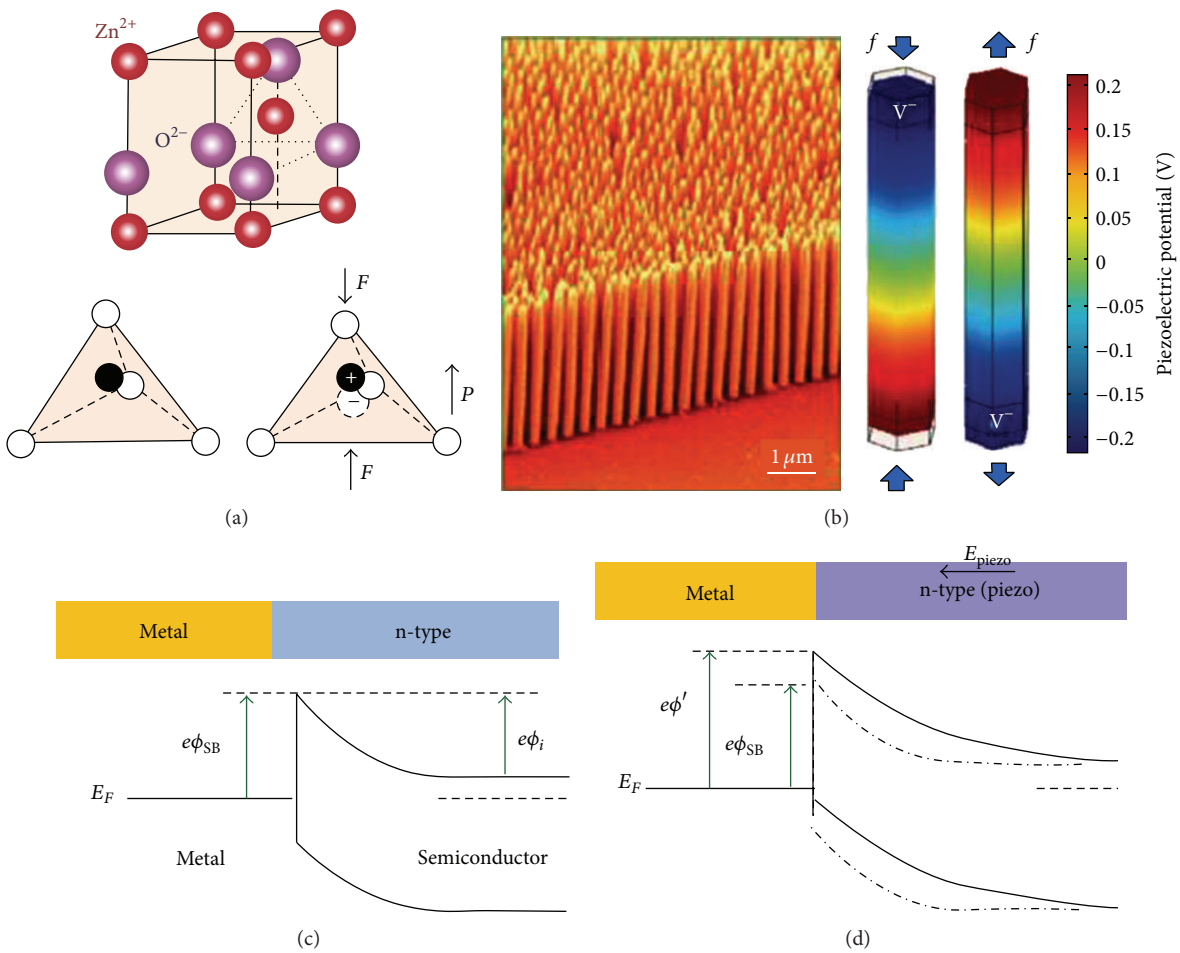

FIGURE 6: Piezopotential in wurtzite crystal. (a) Atomic model of the wurtzite structured ZnO. (b) Aligned ZnO nanowire arrays by solution based approach. Numerical calculated distribution of piezoelectric potential along a ZnO NW under axial strain. The growth direction of the NW is c-axis. The dimensions of the NW are $L = 600$ nm and $a = 25$ nm; the external force is $f_y = 80$ nN. (c) Band diagram of a Schottky-contacted M-S (n-type) interface. (d) Band diagram of the Schottky-contacted after applying a strain in the semiconductor. The piezopotential created in the semiconductor has a polarity with the end in contacting with the metal being low [62, 76]. Copyright 2012, John Wiley and Sons.

Besides, the UV illumination induces the removal of the absorbed O_2 at the SB and thus decreases the barrier height and width, which promotes the improvement of the sensitivity.

Cheng et al. [67] fabricated the UV sensor with a single ZnO NW; they demonstrated the high sensitivity and fast recovery speed of the SB as high performance UV-SCZNS. Under a UV light ($\lambda = 365$ nm, $P = 7.6$ mW/cm^2), the sensitivity, photocurrent gain, and on/off ratio are ~2.6 $\times 10^3$ A/W, ~8.5 $\times 10^3$, and ~4 $\times 10^5$, respectively. The relevant time constant is as short as 46 ms, and the recovery time is 0.28 s when photocurrent decreases by 3 orders of magnitude. The fast recovery speed of UV-SCZNS is due to the following reason: the photocurrent of NW SB has more sensitive response to the amount of reabsorbed O_2^- and relaxed holes in SB interface, and the relaxation speed of holes in SB interface is faster than that on the NW surface.

3.3.2. Piezotronic Effect Enhanced UV-SCZNSs. Zhang et al. [68] fabricated a UV sensor based on the unique crystalline structure of the ZnO-CdS core-shell NW, and they studied the piezophototronic effect on the performance of the sensor under UV light illumination ($\lambda = 372$ nm and $P = 0.636\,\mu$W/cm^2). They find that the UV sensor had a compressive strain-dependent I-V characteristic (Figure 8). The absolute current of the sensor under a 2 V positive bias increases gradually from 12.9 to 144 nA, as the strain of 0% to −0.31% is applied. The sensitivity of the strained ZnO-CdS NW-based sensor is largely enhanced by more than 10 times compared to that of the unstrained NW. The reason is that both the SBHs at the source and drain contacts decrease with increased compressive strains.

Lu et al. [69] also studied the piezoelectric effect on the response of the ZnO/Au Schottky junction UV detector. The sensitivity increases 5 times when applying a 0.58% tensile strain (Figure 9) on the sensor. The enhancement is due to the

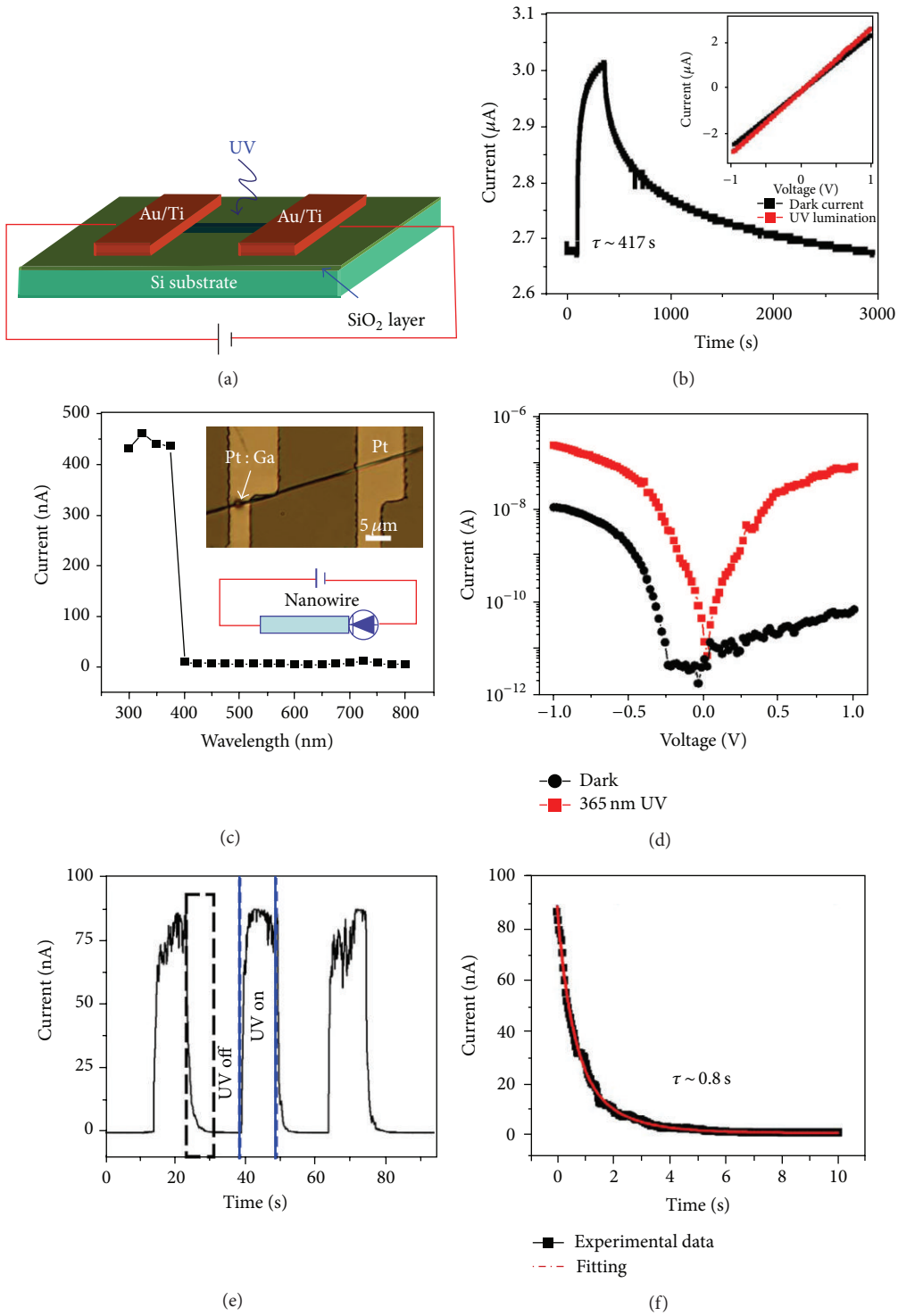

FIGURE 7: (a) Schematic of a ZnO NW UV sensor structure with ohmic-contacted. (b) Schematic of a ZnO NW UV sensor structure with ohmic-contact, when illuminated by 30 μW/cm^2 UV source (365 nm). The inset shows the corresponding I-V characteristics in dark and under UV illumination. (c) Photon-response spectrum of the ZnO NW UV sensor as a function of wavelength of incident light. Upper inset is an optical image of Schottky-contacted UV sensor. Lower inset shows the schematic structure of the device. (d) I-V characteristics of a sensor both in the dark (black cycle) and under 365 nm UV illumination (red rectangle). (e) Time dependence of the photocurrent growth and decay under periodic illumination of the 365 nm UV light on the device. The bias on the device is 1 V. (f) Experimental curve (black) and fitted curve (red) of the photocurrent decay process [59]. Copyright 2009, AIP Publishing LLC.

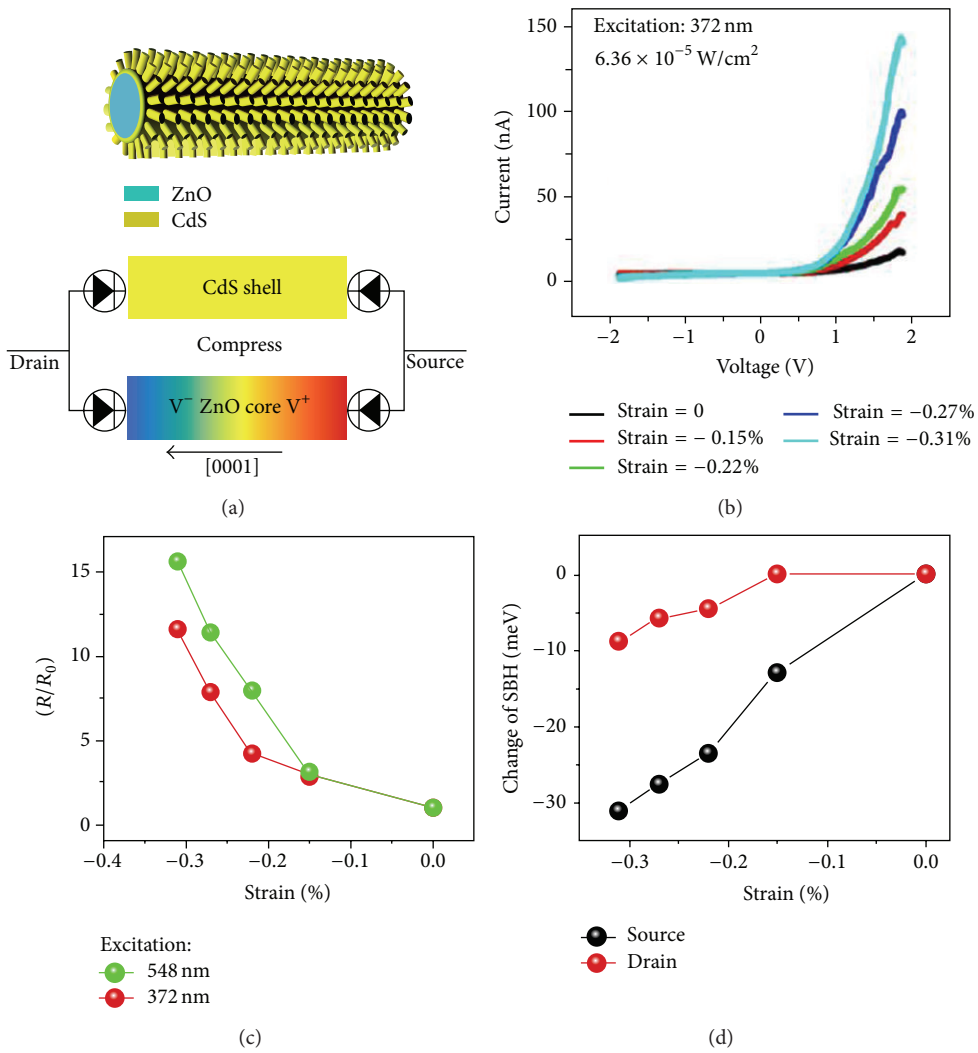

Figure 8: (a) Three-dimensional structure model of a ZnO-CdS core shell wire, showing the structure relationship between ZnO wire core and CdS nanowire array shell. (b) Typical *IV* characteristics of a single ZnO-CdS wire-based device under different compressive strains, excited by UV light centered at 372 nm. (c) The change of responsivity under compressive strains, excited by green light centered at 548 nm and UV light centered at 372 nm; R_0 is set as responsivity under zero strain. (d) The derived change in SBH as a function of compressive strains using the thermionic emission diffusion model. Black curve and red curve are the SBH change for source contact and drain contact at a source drain bias of $V = 2$ and -2 V, respectively [68]. Copyright 2012, American Chemical Society.

charges redistribution induced by piezoelectric polarization at the ZnO/Au interface.

3.4. Gas-SCZNSs

3.4.1. O_2-SCZNSs and CO-SCZNSs. Wang's group demonstrated that the sensitivity of the gas-SCZNSs is several orders higher than the gas-OCZNSs by utilizing the Schottky-contacted structure. Wei et al. [70] compared the performance of the OCZNSs and SCZNSs (Figures 10 and 11). They measure the device in N_2 and O_2 ambient at 275°C, and the linear *I-V* curve shows an excellent ohmic-contacted characteristic (Figure 10(a)). The devices possess a larger resistance in O_2 atmosphere since the chemisorbed O_2 species create a surface electron-depletion layer on the ZnO NW surface. The highest sensitivity of ohmic-contacted device is only 4.8% with a response time of 500 s under 275°C, which indicates that compensating the surface defects can only slightly decrease the conductance. They measured the conductance performance of the SCZNSs at different temperature in N_2 atmosphere and in O_2 atmosphere, and the conductance for both forward and reverse bias modes was decreased because of the electron-depletion layer forming on the ZnO NW surface. Compared to the ohmic-contacted analogues, the Schottky-contacted device has higher sensitivities. Under the forward bias, the highest sensitivity of 257% is obtained at the response time of 500 s and temperature of 275°C, which is 54 times higher than 4.8% of the ohmic-contacted sensors under the same sensing conditions. While under the reverse bias, the highest sensitivity of 3235% is obtained for the Schottky-contacted device and the sensitivity was 27 times higher than that of the same device under forward

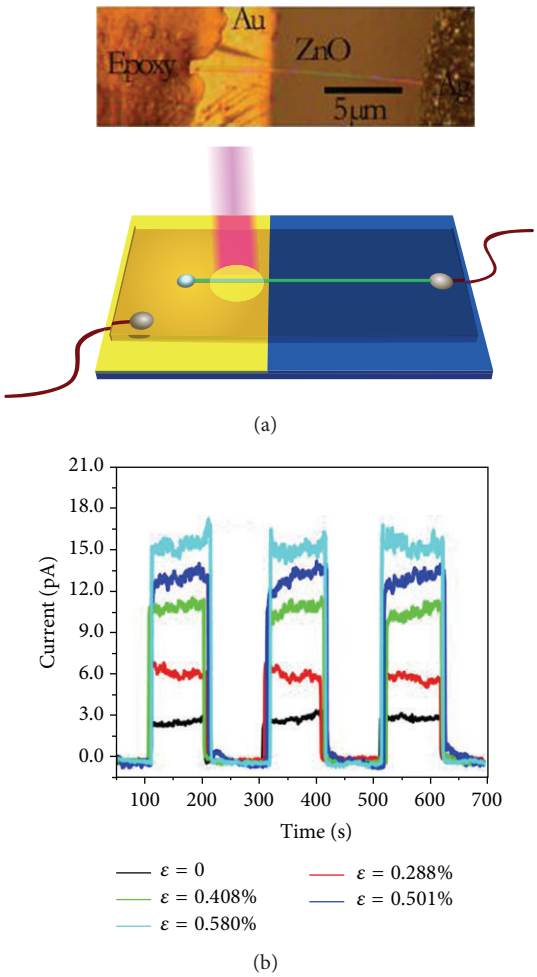

Figure 9: (a) Optical image (top) and schematic of the fabricated device (bottom). (b) Strain effect on the photo response characteristics [69]. Copyright 2014, American Chemical Society.

bias and 1085 times higher than that of the ohmic-contacted device.

CO sensing properties are also investigated, as shown in Figure 11. The blue region is O_2 conditioning and N_2 purge process, while the yellow region is the CO sensing for duration of 60 min. It shows that the sensitivity increases with the increase of CO concentration, consistent with the previous reports [71, 72]. The highest sensitivity of 32 000% for the CO-SCZNS under reverse bias mode is obtained in the 400 ppm CO concentration at 275°C, while the sensitivity of the ohmic-contacted device is only 3.8% at the same condition. Comparing with the ohmic-contacted device, the great success of the Schottky-contacted device relies on the modulation of the SBH through adsorption and removal of the negatively charged species.

3.4.2. Humidity-SCZNSs. Herrán et al. [73] presented a room temperature Ag/ZnO Schottky diode for relative humidity (RH) monitoring. The sensor can detect the RH based on the adsorption of the water molecules on the NR surface and the reduction of the majority of carriers in the conduction band of the semiconductor. The sensitivity shows a logarithmic relation between 20% and 75% of RH and the response time is about 5 s; this is due to the physical behavior of the Schottky diode according to the M-S junction between the ZnO and the Ag.

3.4.3. Piezotronic Effect Enhanced Gas-SCZNSs

(1) Piezotronic Effect Enhanced O_2-SCZNSs. Niu et al. [74] studied the piezotronic effect on the O_2-SCZNSs. The typical SEM image of the ZnO NWs, optical image, and a schematic of the measurement setup are shown in Figure 12. The electrical performance of the device is measured after a UV lamp (λ = 254 nm and P = 23 W) treatment. Under the 1 V bias, the current drops with the increase of either oxygen pressure or tensile strain, whereas under the bias of −1 V, the current slightly decreases with the tensile strain, while it greatly decreases with the increased O_2 pressure. In the 700 Torr O_2 pressures and applying 0 to 0.2% tensile strain, under the 1 V bias, the relative current enhances from −55.4% to −75.4%, while under the −1 V bias, the relative current increases from −87.3% to −93%, respectively. It is due to the adsorption of O_2, an electron-depletion layer is formed on the ZnO NW surface and reduces the carrier density in the NW, and the O_2 adsorbed around the Schottky-contacted area increases the SBH, which reduces the overall current [75–77]. Besides, by applying a tensile strain, the already downward trend to O_2 can be further enhanced by piezotronic effect.

(2) Piezotronic Effect Enhanced Humidity-SCZNSs. Hu et al. [78] investigated the piezotronic effect on the performances of the humidity-SCZNSs. They fabricate the Schottky-contacted devices and detect the performance of the humidity sensor (Figure 13). The experiment is carried out at a fixed bias of 2.8 V under different humidity and strain conditions. By comparing the relative current response to different RH under each certain strain condition, it is concluded that the current increases with the increase of compressive strain and the decrease of RH. Furthermore, the slopes of curves become deeper with increasing the strain, which means that the relative sensitivity of humidity sensors is improved by the piezotronic effect. In the ZnO NW humidity sensor, a −0.22% compressive strain can optimize the performances by achieving the largest responsivity of 1,240%. These results demonstrate that the piezotronic effect can enhance the performance of humidity sensors at different RH and improve the sensing resolution by significantly enlarging the current differences between two RHs under certain strain condition.

3.5. Bio/Chemical-SCZNSs

3.5.1. Bio-SCZNSs. Yeh et al. [79] fabricated both the Schottky-contacted and ohmic-contacted ZnO NW devices. The conductance performance of the ohmic-contacted devices is shown in Figure 14. No obvious signal is observed when the concentration of the charged target molecules is lower than 800 μg/mL, probably because the conductance of the ZnO NW is so high that the introduction of surface-absorbed molecules cannot change the conductance of the

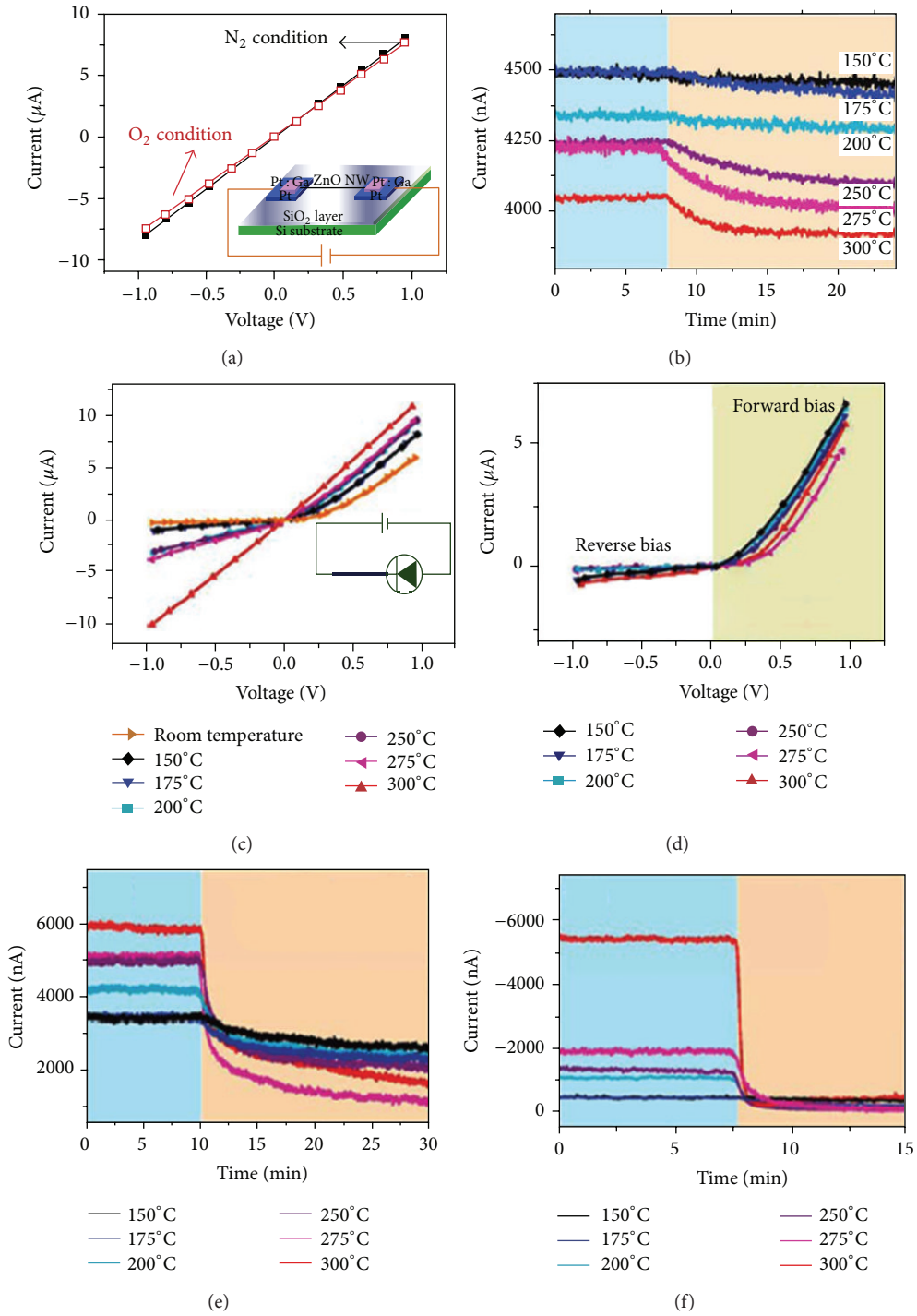

FIGURE 10: (a) *I-V* curves measured for the ohmic-contacted device in N_2 and O_2 atmospheres at 275°C. Inset shows the schematic of a typical ohmic-contacted gas sensor. (b) The response curves of the oxygen detection recorded at different temperatures, ranging from 150 to 300°C, for the ohmic-contacted device. The blue background denotes that the sensor was in the N_2 atmosphere and the pink background in the O_2 atmosphere. (c) *I-V* curves of the Schottky-contacted device measured at different temperatures in N_2 atmosphere. Inset shows the equivalent circuit of a Schottky-contacted gas sensor. (d) *I-V* curves of the Schottky-contacted device measured at different temperatures in O_2 atmosphere. (e) Response curves of the oxygen detection recorded at different temperatures, ranging from 150 to 300°C, for the Schottky-contacted device operated under forward bias. (f) Response curves of the oxygen detection recorded at different temperatures, ranging from 150 to 300°C, for the Schottky-contacted device operated under reverse bias [70]. Copyright 2009, American Chemical Society.

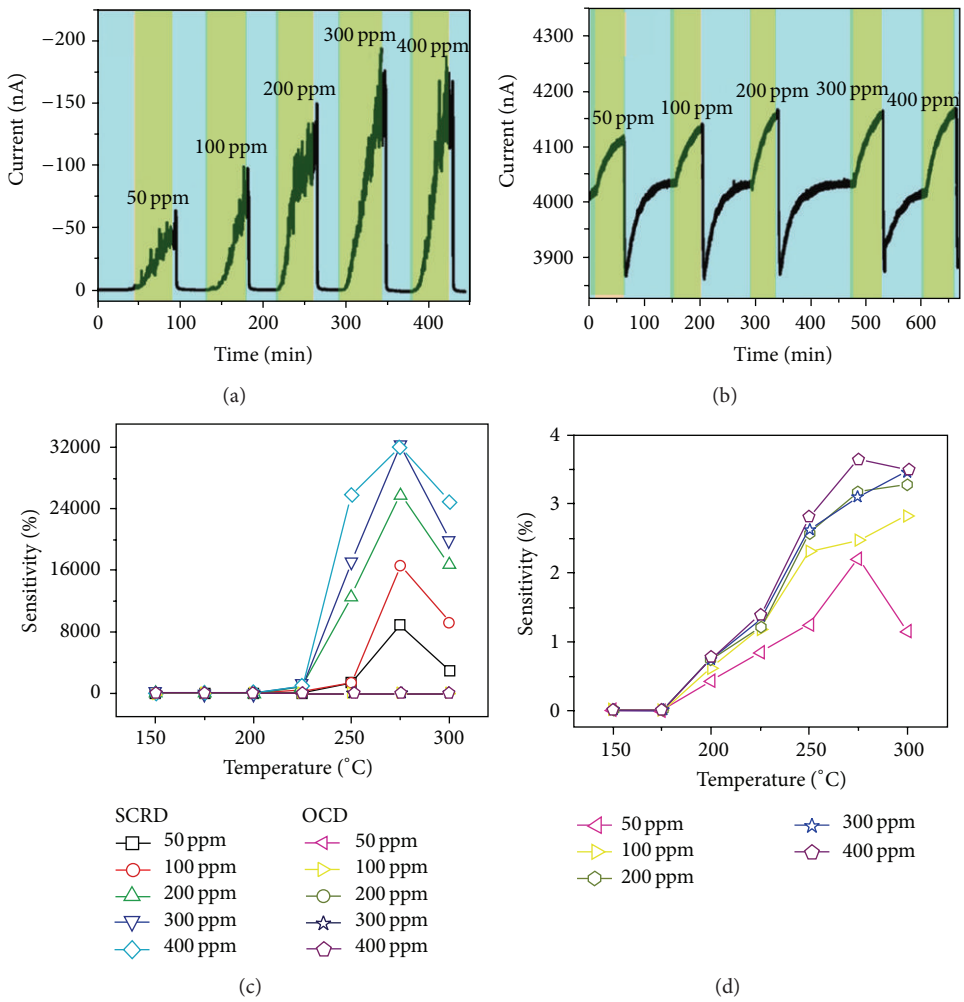

Figure 11: Response curves of the CO detection recorded at 275°C with the device exposed to increased concentration of CO: (a) for the Schottky-contacted device under reverse bias and (b) for the ohmic-contacted device. (c) Sensitivity versus system temperature for CO sensing at a response time of 1 h as a function of the CO concentration. (d) Enlarged plot of the data from panel (c) for the ohmic-contacted device [70]. Copyright 2009, American Chemical Society.

NW significantly. However, the Schottky-contacted device shows a fast response and distinctly current change for different concentrations. The devices are immersed in DI water as the signal baseline for measuring the conductance, and in this case, the negatively charged molecules absorbed around the SB area increase the barrier height and decrease the current. In contrast, when introduced positively charged molecules increase the current. The performance of the biosensor is largely controlled by the characteristic of the SBH, which can get different effects for detecting positively and negatively charged molecules.

3.5.2. Piezotronic Effect Enhanced Bio/Chemical-SCZNSs

(1) Piezotronic Effect Enhanced pH-SCZNSs. Pan et al. [17] demonstrated the piezotronic effect on the pH-SCZNSs, as shown in Figure 15. They fabricate the device by using the silver paste to get the Schottky-contact, and in order to prevent the two silver electrodes from contacting with the buffer solutions, the two electrodes are fully covered by a layer of epoxy. The signal of the pH sensor decreases step-by-step with discrete changing in pH from 3 to 12 under no strain condition, and the stable and repeatable performances of the pH sensor are detected in solutions (pH = 5 and pH = 12). The reason for the decrease in different pH value is as follows: at high pH, OH^- correspondingly depletes the electron carriers and decreases the conductance, while at low pH, H^+ increases the electron carriers in the n-type ZnO NW and the conductance. When applying a 0.5 V bias voltage, the signal level of a nonstrain sensor is only 1.2 nA in the buffer solution with pH = 5. However, when a −0.92% compressive strain is applied on the device, the current jumps to 1.75 μA, and equivalently the current increases by about 1500 times in magnitude. Under externally applied strain in different pH value buffer solutions, the signal current increases with applied strain, because the SBH is changed by the strain, and the relative changes of the SBH (ΔSBH) can be calculated according to Yang et al.'s work

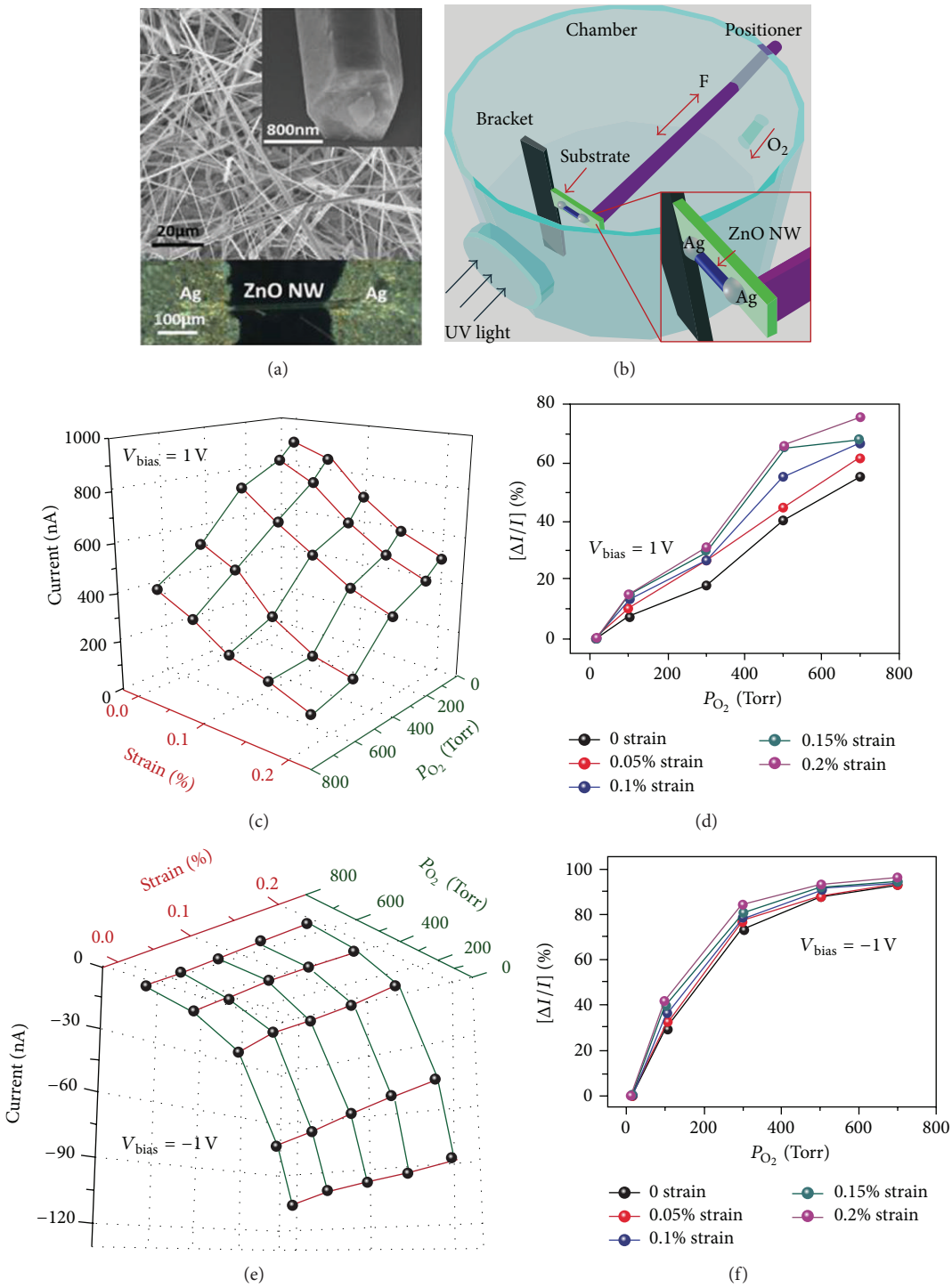

FIGURE 12: Piezotronic effect on the performance of an individual ZnO NW-based room temperature oxygen sensor (a) SEM images of ZnO NWs. The inset is a high-magnification image of an individual wire (top right) and optical microscopy image of a ZnO NW oxygen sensor device (bottom). (b) Schematic of the measurement setups for studying the piezotronic effect in a ZnO NW oxygen sensor (c) 3D graph depicting the current response of the ZnO NW oxygen sensor under different strains and oxygen pressures at a bias voltage equal to 1 V. (d) Magnitude of relative current change with oxygen pressure under different tensile strain from 0% to 0.2% at a bias voltage of 1 V. ((e)-(f)) Corresponding results of Figure 12 (c, d) at bias voltage of −1 V [74]. Copyright 2013, John Wiley and Sons.

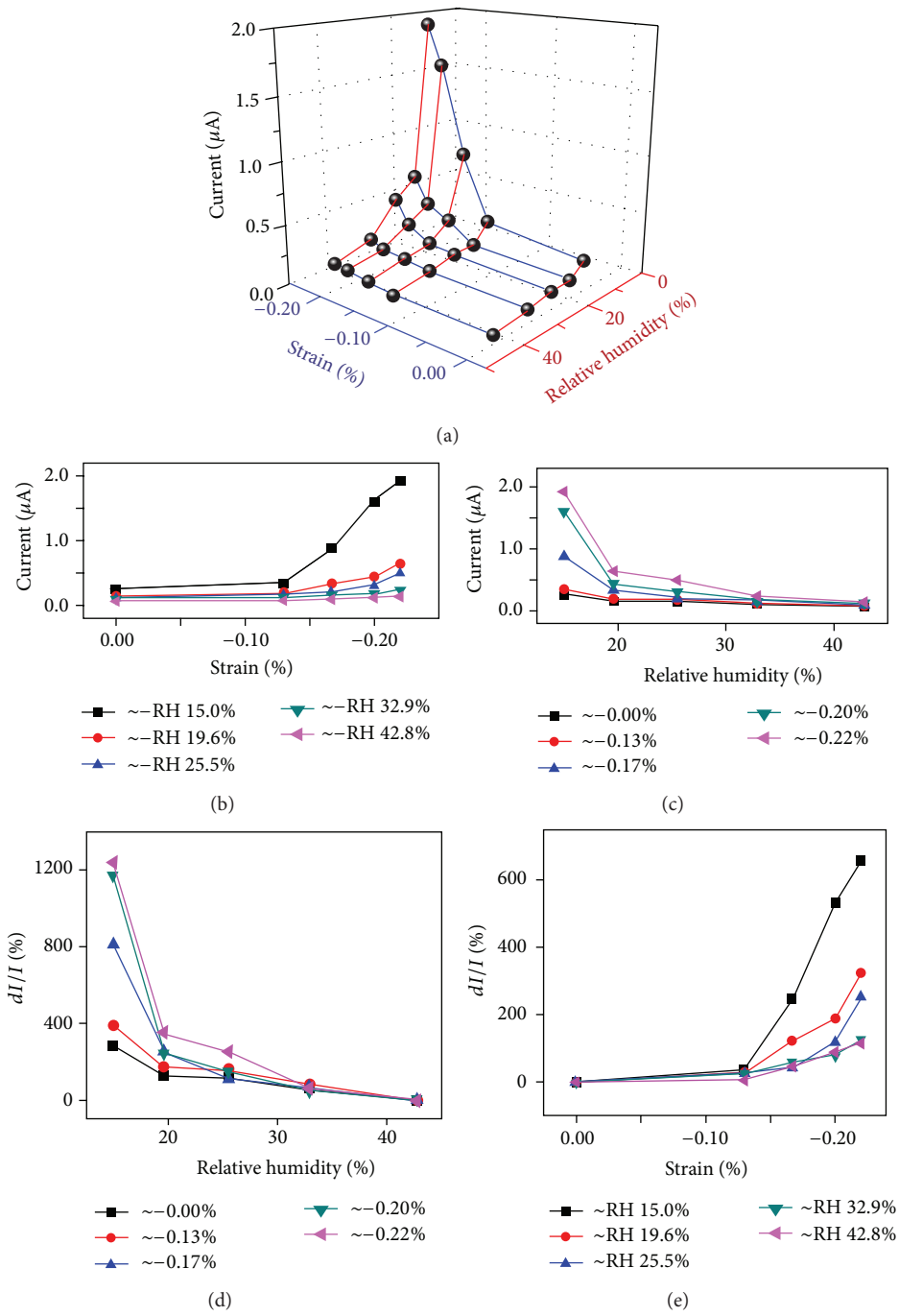

Figure 13: (a) 3D graph depicts the current response of the ZnO NW humidity sensor to strain and relative humidity at a bias voltage of 2.8 V. (b) Absolute current response to different compressive strains, with relative humidity ranging from 15.0% to 42.8%. (c) Absolute current response to different relative humidity, with compressive strains ranging from −0.00% to −0.22%. (d) Indicating the relative changes of current with respect to the value at 42.8% RH, under different compressive strains ranging from −0.00% to −0.22%. (e) Indicating the relative changes of current with respect to the value at 0.0% strain, under different RHs ranging from 15.0% to 42.8% [78]. Copyright 2014, Springer.

[80, 81]. The test results demonstrate that the piezotronic effect can enhance the sensitivity of the SCZNSs.

(2) Piezotronic Effect Enhanced Glucose-SCZNSs. Yu et al. [18] investigated the piezotronic effect on the performances of the glucose-SCZNSs. The fabrication method of the glucose sensor is similar to the pH-SCZNSs [17], while in Yu's research, they decorate the glucose oxidases (GO_x) onto the ZnO NW. It is obvious that the current increases with the incremental compressive strains (Figure 16), at a bias voltage

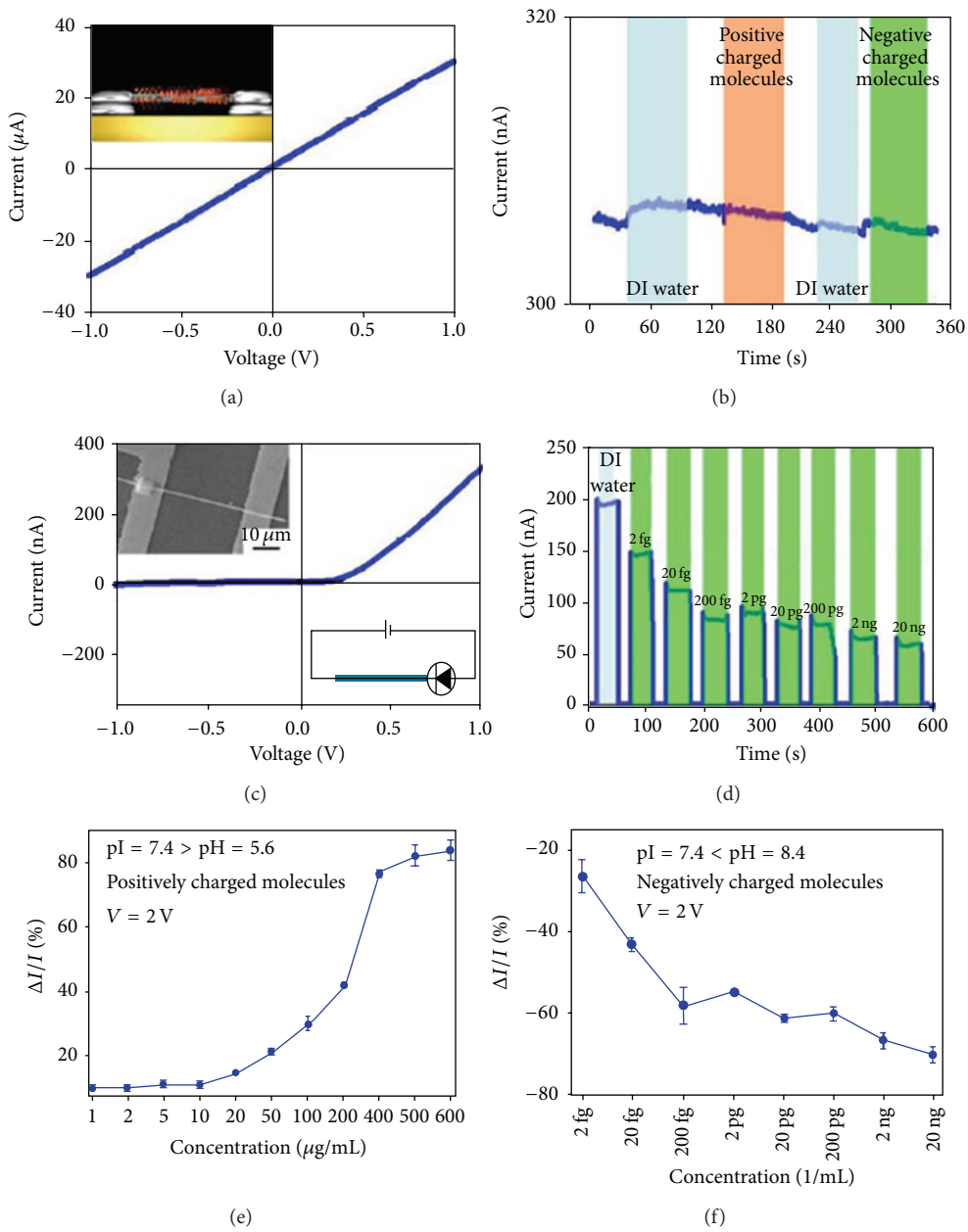

Figure 14: The ohmic-contacted biosensor was fabricated using a single-crystal ZnO NW that shows little response to the biomolecules. (a) Pt-Ga was deposited by FIB on both ends of the NW to form ohmic-contact (inset), as proven by its corresponding I-V curve. (b) When either positively charged molecules or negatively charged molecules are introduced, the electrical signal of the device shows little change. (c) SEM image of a Schottky-contacted biosensor is shown in the upper-left inset. The I-V curve shows a typical Schottky characteristic. (d) A fast response and distinct current variations can be seen when the sensor is exposed to a series of concentrations of negatively charged molecules (pI 7.4 < pH 8.4). (e) When the molecules are positively charged (pI 7.4 > pH 5.6), the conductance of the device increases. (f) The negatively charged molecules result in a decrease in conductance [79]. Copyright 2009, John Wiley and Sons.

of 1.8 V; as a −0.79% compressive strain is applied, the current increases from 0.15 μA to more than 25 μA, which is about 150 times larger in magnitude. The output signal of a strain-free ZnO NW glucose sensor clearly increases stepwise with gradually adding glucose into the solution, measured at a fixed bias of 2 V.

Furthermore, they studied the response of the glucose sensors to continuously changed glucose concentrations and compressive strains. It is clear that the current increases stepwise with the glucose concentrations and the relative change in current is around 130% by adding 1.5 g/L glucose without strain. The current difference between two certain glucose concentrations is obviously increased when applying more compressive strain, and this relative change in current has the largest value more than 300% and mostly relative change in current is around 150%. These results indicate that

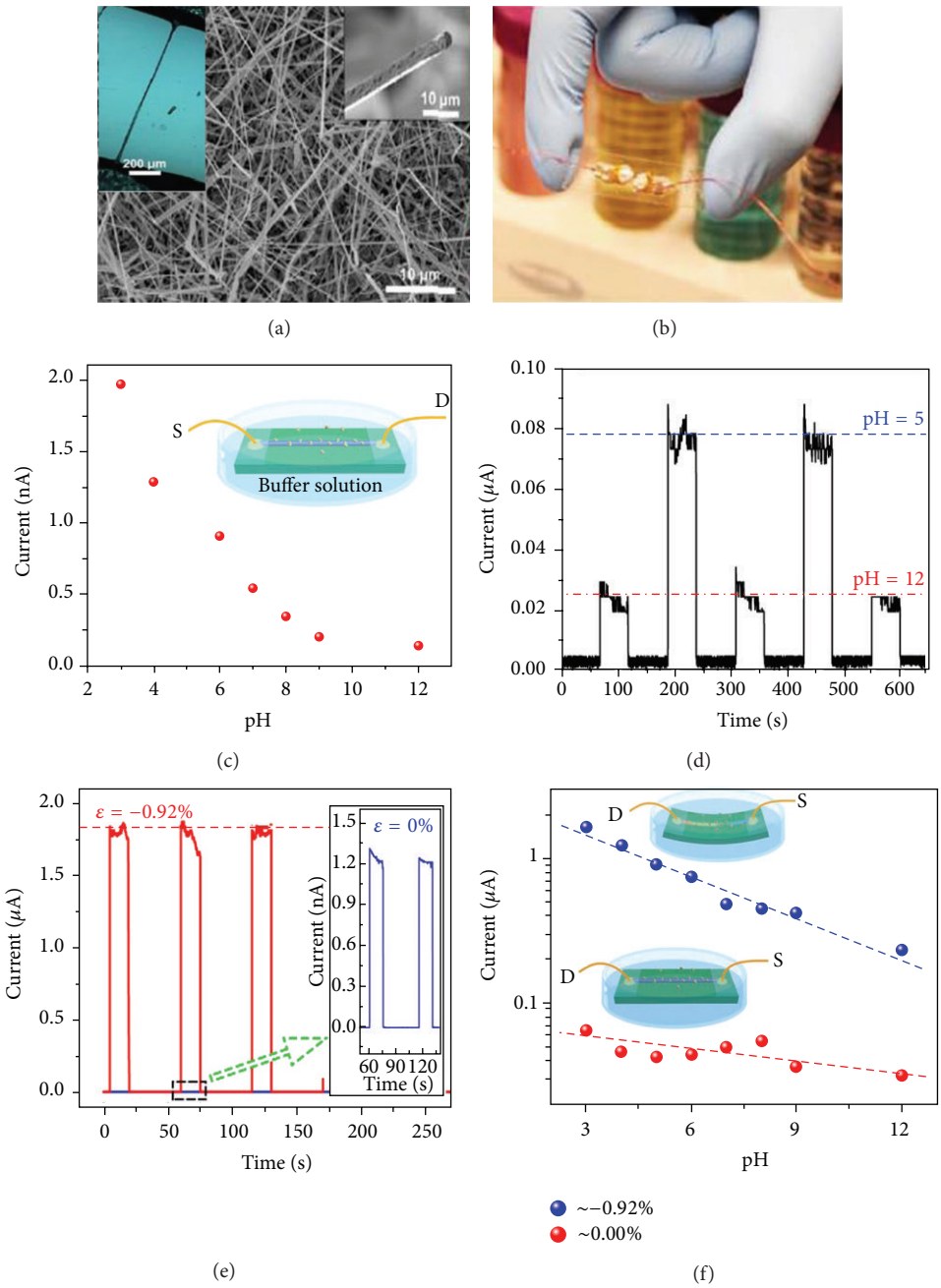

Figure 15: (a) SEM image of the morphology of the as-synthesized ZnO NWs. The insert is a high-magnification image of an individual wire and Optical microscopy. (b) Digital image of a ZnO NW pH sensor. (c) The response of the sensor to the pH varying from 3 to 12, no external strain was applied, just like traditional NW based sensors. (d) The repeatability of the ZnO sensor pH sensor at pH 5 and 12. The signal level and the sensitivity of the sensor are increased by the piezotronics effect. (e) The output signal of a sensor in a buffer solution with pH = 5 when the strain is "off" (blue) and "on" (red). The signal is increased about 1500 times when a compressive strain of $\varepsilon = -0.92\%$ was applied. (f) The response of the sensor to the pH varying from 3 to 12, when the device is strain off (red) and on (blue) [17]. Copyright 2013, American Chemical Society.

the relative change of output signals in applying strains case is even much larger than that in the adding glucose case. The sensitivity and sensing resolution of the glucose sensor is generally enhanced by the piezotronic effect.

(3) Piezotronic Effect Enhanced Protein-SCZNSs. Yu et al. [19] also demonstrated the piezotronic effect on the performances of the protein-SCZNSs, as shown in Figure 17. The device is fabricated similar to the aforementioned pH-SCZNSs [17], by adding 0.01 mL of gold nanoparticles-anti immunoglobulin G conjugates (Au NP-anti-IgG) colloidal solution on the NW, and then the NW is modified with a blocking buffer (BB), 0.1% fish gelatin, and 1% Bovine Serum Albumin (BSA). BB can efficiently block the nonspecific binding of IgGs

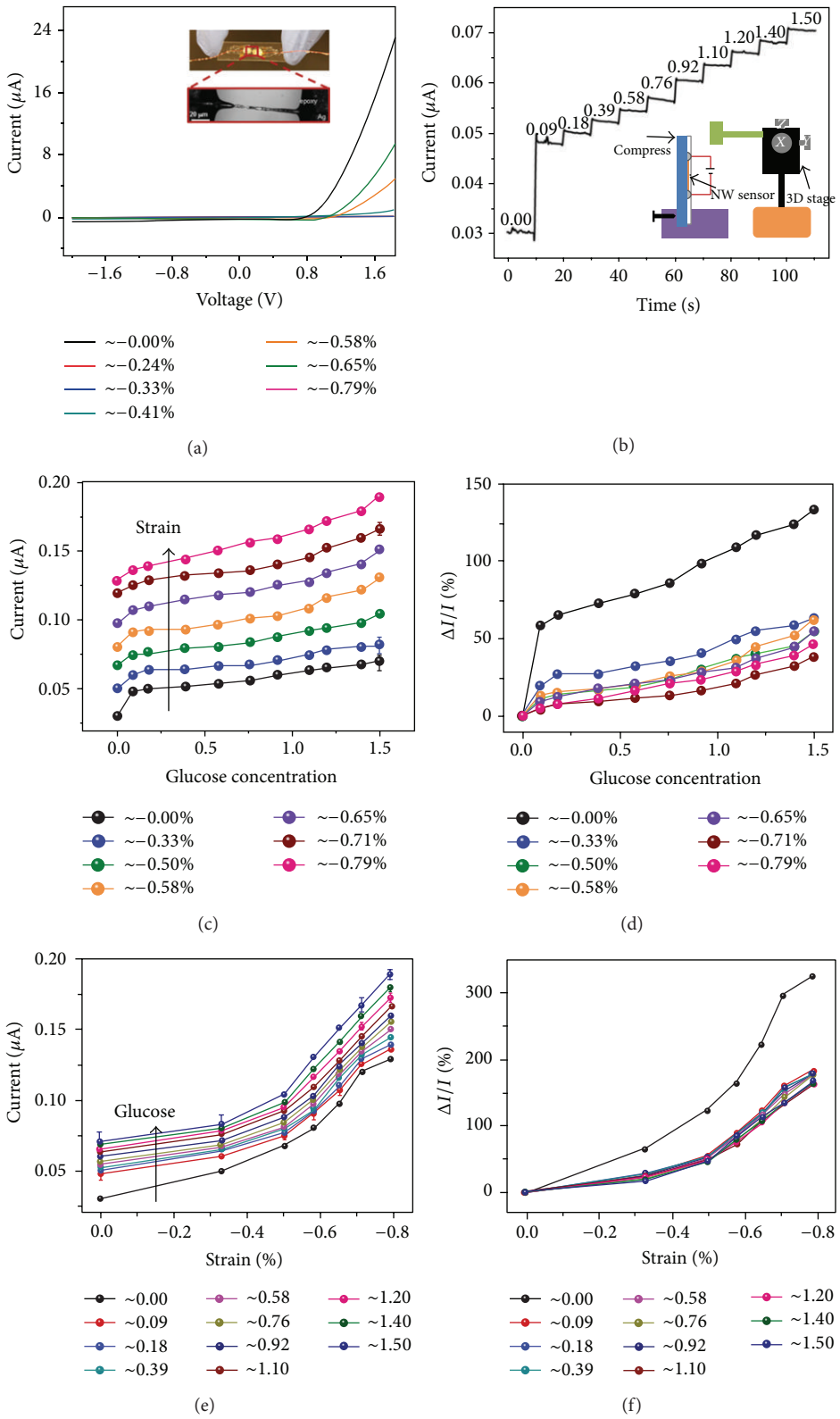

FIGURE 16: (a) *I-V* characteristics of a ZnO NW glucose sensor under different compressive strains, no glucose added. The inset shows a digital image and an optical microscopy image of the ZnO NW glucose sensor. (b) *I-t* characteristics of another ZnO NW glucose sensor in different glucose concentrations, no external strains applied. The inset presents a schematic of the experiments setup. (c)-(d) Absolute and relative current response of the ZnO NW glucose sensor in different glucose concentrations, with compressive strain ranging from 0 to −0.79%, respectively. (e)-(f) Absolute and relative current response of the ZnO NW glucose sensor under different compressive strains, with glucose concentration ranging from 0 to 1.50 g/L, respectively [18]. Copyright 2013, John Wiley and Sons.

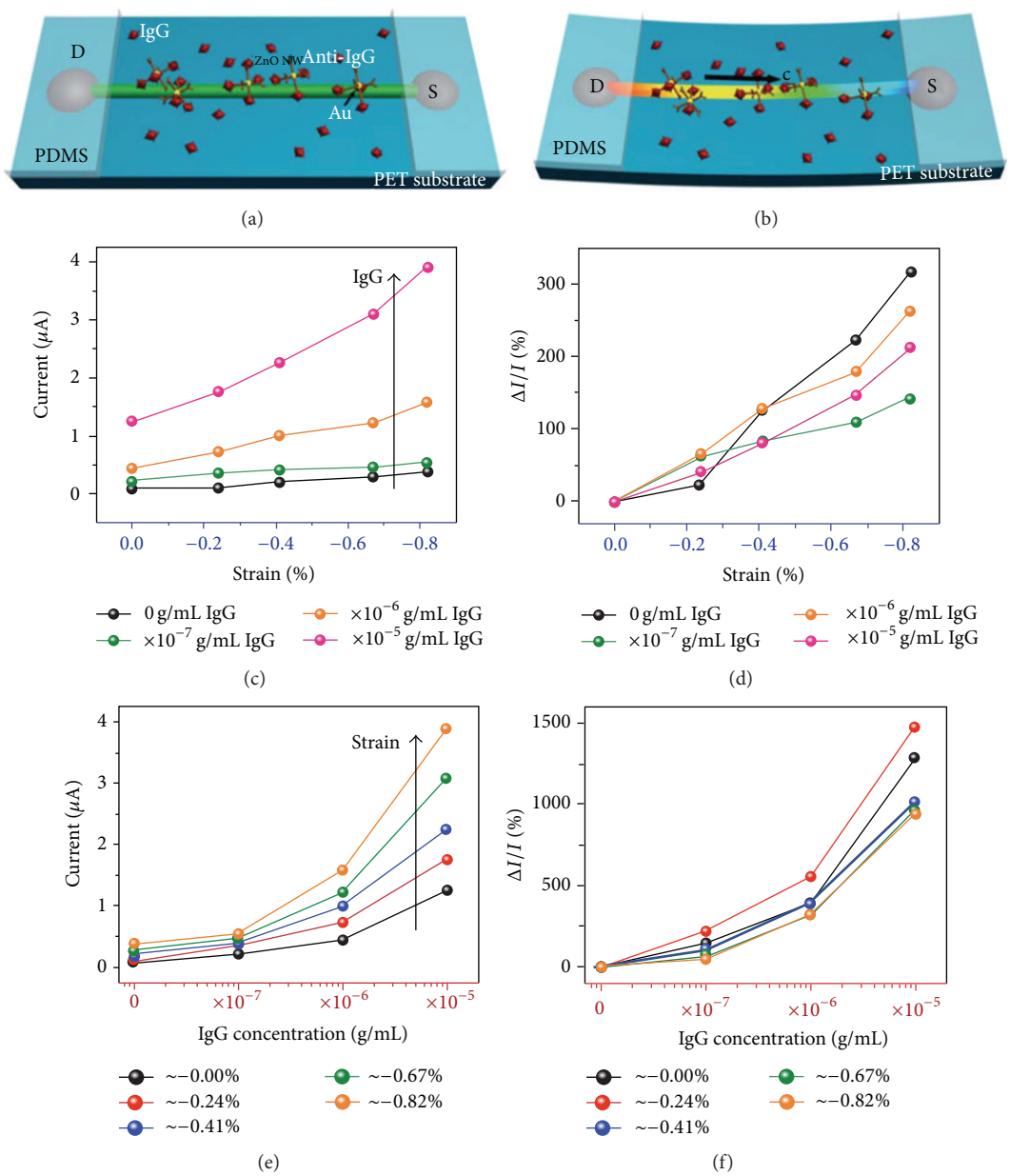

FIGURE 17: (a) Gold nanoparticle anti-IgG surface functionalized ZnO NW protein sensor bonding with target protein IgG. (b) ZnO NW protein sensor under compressive strain. ((c)-(d)) Absolute and relative current response of ZnO NW protein sensor under different compressive strains, with IgG concentration ranging from 0 to 1×10^{-5} g/mL, respectively. ((e)-(f)) Absolute and relative current response of ZnO NW protein sensor at different IgG concentrations, with compressive strain ranging from 0 to −0.82%, respectively [19]. Copyright 2012, Royal Society of Chemistry.

to the devices [82]. Therefore, treating the device with BB can effectively decrease the undesirable response from the nonspecific binding to the device and is essential for the specific function of the sensor.

It is obvious that current increases with increasing the IgG concentrations or compressive strains. The difference between currents related to two adjacent IgG concentrations is enlarged as the strain increases, which is the result from the nonlinear I-V transport properties controlled by the SB at the contacts of the metal-semiconductor-metal (M-S-M) structure. It can also be seen that, at a fixed IgG concentration, the larger the strain applied, the higher the output current observed. These results obviously show that the piezotronic effect can improve the resolution, the detection limit, and the sensitivity of the protein-SCZNSs.

In general, the SCZNSs exhibit higher sensitivity and faster response than the OCZNSs. For SCZNSs, the adsorption of a few molecules at the junction area could effectively change the local barrier height. The piezotronic efect [83, 84] play a dominant role in optimizing enhance the performance of the SCZNSs.

4. Conclusions and Outlook

In this paper, we introduce ZnO NW sensors based on the ohmic-contacted and Schottky-contacted structure, the working principle, and performance enhancement of the OCZNSs and SCZNSs. For the OCZNSs, the current change is regarded as the result of the "gate voltage" modulating through the external adsorbed molecules. The performance of this kind of devices is usually affected by the bias and gate voltage, the decorated surface, and the size of ZnO NWs. For SCZNSs, the output signals of these devices could be optimized by several orders of magnitudes higher than that of the OCZNSs. By utilizing the piezotronic effect to modulate the SBH, the extremely high sensitivity can be obtained.

The ZnO NW devices should be further optimized in sensitivity to detect force, heat, light, humid, gas, and so forth, and the piezoelectric material system, single NW device, or integrated NW sensor arrays will be further investigated in other research fields. Undoubtedly, the piezotronic-enhanced Schottky-contacted sensors will have potentially important applications in photoelectric detection, environment monitoring, health monitoring, and robotics.

Conflict of Interests

The authors declare that there is no conflict of interests regarding the publication of this paper.

Acknowledgments

The authors acknowledge the support from the "Thousand Talents" program for pioneer researcher and its innovation team, China, President Funding of the Chinese Academy of Sciences, National Natural Science Foundation of China (nos. 51272238, 21321062, 51432005, and 61405040), the Innovation Talent Project of Henan Province (no. 13HASTIT020), Talent Project of Zhengzhou University (ZDGD13001), and Surface Engineering Key Lab of LIPCAST.

References

[1] A. L. Briseno, T. W. Holcombe, A. I. Boukai et al., "Oligo- and polythiophene/ZnO hybrid nanowire solar cells," *Nano Letters*, vol. 10, no. 1, pp. 334–340, 2010.

[2] N. P. Dasgupta and P. Yang, "Semiconductor nanowires for photovoltaic and photoelectrochemical energy conversion," *Frontiers of Physics*, vol. 9, no. 3, pp. 289–302, 2014.

[3] Y. Hu, J. Zhou, P. H. Yeh, Z. Li, T. Wei, and Z. L. Wang, "Supersensitive, fast-response nanowire sensors by using Schottky contacts," *Advanced Materials*, vol. 22, no. 30, pp. 3327–3332, 2010.

[4] A. A. Iliadis, R. D. Vispute, T. Venkatesan, and K. Jones, "Ohmic metallization technology for wide band-gap semiconductors," *Thin Solid Films*, vol. 420-421, pp. 478–486, 2002.

[5] A. Inumpudi, A. Iliadis, S. Krishnamoorthy, S. Choopun, R. Vispute, and T. Venkatesan, "Pt–Ga Ohmic contacts to n-ZnO using focused ion beams," *Solid-State Electronics*, vol. 46, no. 10, pp. 1665–1668, 2002.

[6] K. Ip, Y. W. Heo, K. H. Baik, D. P. Norton, S. J. Pearton, and F. Ren, "Carrier concentration dependence of Ti/Al/Pt/Au contact resistance on n-type ZnO," *Applied Physics Letters*, vol. 84, no. 4, p. 544, 2004.

[7] S. T. Jun and G. M. Choi, "CO gas-sensing properties of ZnO/CuO contact ceramics," *Sensors and Actuators B: Chemical*, vol. 17, no. 3, pp. 175–178, 1994.

[8] B. M. Kulwicki, "Humidity sensors," *Journal of the American Ceramic Society*, vol. 74, no. 4, pp. 697–708, 1991.

[9] Y. Liu, C. R. Gorla, S. Liang et al., "Ultraviolet detectors based on epitaxial ZnO films grown by MOCVD," *Journal of Electronic Materials*, vol. 29, no. 1, pp. 69–74, 2000.

[10] S. R. Morrison, "Semiconductor gas sensors," *Sensors and Actuators*, vol. 2, no. 205, pp. 329–341, 1982.

[11] M. Ahn, K. Park, J. Heo et al., "Gas sensing properties of defect-controlled ZnO-nanowire gas sensor," *Applied Physics Letters*, vol. 93, no. 26, 2008.

[12] A. B. Artyukhin, M. Stadermann, R. W. Friddle, P. Stroeve, O. Bakajin, and A. Noy, "Controlled electrostatic gating of carbon nanotube FET devices," *Nano Letters*, vol. 6, no. 9, pp. 2080–2085, 2006.

[13] M. Curreli, C. Li, Y. H. Sun et al., "Selective functionalization of In_2O_3 nanowire mat devices for biosensing applications," *Journal of the American Chemical Society*, vol. 127, no. 19, pp. 6922–6923, 2005.

[14] Z. Fan and J. G. Lu, "Gate-refreshable nanowire chemical sensors," *Applied Physics Letters*, vol. 86, no. 12, Article ID 123510, 2005.

[15] H. Kind, H. Yan, B. Messer, M. Law, and P. Yang, "Nanowire ultraviolet photodetectors and optical switches," *Advanced Materials*, vol. 14, no. 2, pp. 158–160, 2002.

[16] X. Tang, S. Bansaruntip, N. Nakayama, E. Yenilmez, Y. Chang, and Q. Wang, "Carbon nanotube DNA sensor and sensing mechanism," *Nano Letters*, vol. 6, no. 8, pp. 1632–1636, 2006.

[17] C. Pan, R. Yu, S. Niu, G. Zhu, and Z. L. Wang, "Piezotronic effect on the sensitivity and signal level of Schottky contacted proactive micro/nanowire nanosensors," *ACS Nano*, vol. 7, no. 2, pp. 1803–1810, 2013.

[18] R. Yu, C. Pan, J. Chen, G. Zhu, and Z. L. Wang, "Enhanced performance of a ZnO nanowire-based self-powered glucose sensor by piezotronic effect," *Advanced Functional Materials*, vol. 23, no. 47, pp. 5868–5874, 2013.

[19] R. Yu, C. Pan, and Z. L. Wang, "High performance of ZnO nanowire protein sensors enhanced by the piezotronic effect," *Energy & Environmental Science*, vol. 6, no. 2, p. 494, 2013.

[20] R. K. Gupta and F. Yakuphanoglu, "Photoconductive Schottky diode based on Al/p-Si/SnS_2/Ag for optical sensor applications," *Solar Energy*, vol. 86, no. 5, pp. 1539–1545, 2012.

[21] N. J. Ku, J. H. Huang, C. H. Wang, H. Fang, and C. Liu, "Crystal face-dependent nanopiezotronics of an obliquely aligned InN nanorod array," *Nano Letters*, vol. 12, no. 2, pp. 562–568, 2012.

[22] K. Momeni and H. Attariani, "Electromechanical properties of 1D ZnO nanostructures: nanopiezotronics building blocks, surface and size-scale effects," *Physical Chemistry Chemical Physics*, vol. 16, no. 10, pp. 4522–4527, 2014.

[23] Z. L. Wang, "The new field of nanopiezotronics," *Materials Today*, vol. 10, no. 5, pp. 20–28, 2007.

[24] F. M. Zörgiebel, S. Pregl, L. Römhildt et al., "Schottky barrier-based silicon nanowire pH sensor with live sensitivity control," *Nano Research*, vol. 7, no. 2, pp. 263–271, 2014.

[25] Y. Fu, W. L. Zang, P. L. Wang, L. Xing, X. Xue, and Y. Zhang, "Portable room-temperature self-powered/active H_2 sensor driven by human motion through piezoelectric screening effect," *Nano Energy*, vol. 8, pp. 34–43, 2014.

[26] M. L. Seol, J. M. Choi, J. Y. Kim, J. Ahn, D. Moon, and Y. Choi, "Piezoelectric nanogenerator with a nanoforest structure," *Nano Energy*, vol. 2, no. 6, pp. 1142–1148, 2013.

[27] X. D. Wang, "Piezoelectric nanogenerators-harvesting ambient mechanical energy at the nanometer scale," *Nano Energy*, vol. 1, no. 285, pp. 13–24, 2012.

[28] Z. Zhang, Q. L. Liao, Y. H. Yu, X. Wang, and Y. Zhang, "Enhanced photoresponse of ZnO nanorods-based self-powered photodetector by piezotronic interface engineering," *Nano Energy*, vol. 9, no. 284, pp. 237–244, 2014.

[29] J. He, Y. Zhang, J. Liu, D. Moore, G. Bao, and Z. Wang, "ZnS/Silica nanocable field effect transistors as biological and chemical nanosensors," *The Journal of Physical Chemistry C*, vol. 111, no. 33, pp. 12152–12156, 2007.

[30] F. Patolsky and C. M. Lieber, "Nanowire nanosensors," *Materials Today*, vol. 8, no. 4, pp. 20–28, 2005.

[31] Y. Cui and C. M. Lieber, "Functional nanoscale electronic devices assembled using silicon nanowire building blocks," *Science*, vol. 291, no. 5505, pp. 851–853, 2001.

[32] Z. Fan, D. Wang, P.-C. Chang, W. Tseng, and J. G. Lu, "ZnO nanowire field-effect transistor and oxygen sensing property," *Applied Physics Letters*, vol. 85, no. 24, Article 5923, 2004.

[33] P. Andrei, L. Fields, J. Zheng, Y. Cheng, and P. Xiong, "Modeling and simulation of single nanobelt SnO_2 gas sensors with FET structure," *Sensors and Actuators B: Chemical*, vol. 128, no. 1, pp. 226–234, 2007.

[34] A. J. Soares and R. J. Perry, "Modeling and simulation of a single tin dioxide nanobelt FET for chemical sensors," *IEEE Sensors Journal*, vol. 10, no. 2, pp. 235–242, 2010.

[35] R. J. Chen, H. C. Choi, S. Bangsaruntip et al., "An investigation of the mechanisms of electronic sensing of protein adsorption on carbon nanotube devices," *Journal of the American Chemical Society*, vol. 126, no. 5, pp. 1563–1568, 2004.

[36] E. L. Gui, L. Li, K. Zhang et al., "DNA sensing by field-effect transistors based on networks of carbon nanotubes," *Journal of the American Chemical Society*, vol. 129, no. 46, pp. 14427–14432, 2007.

[37] I. Heller, A. M. Janssens, J. Männik, E. D. Minot, S. G. Lemay, and C. Dekker, "Identifying the mechanism of biosensing with carbon nanotube transistors," *Nano Letters*, vol. 8, no. 2, pp. 591–595, 2008.

[38] Y. Cheng, P. Xiong, L. Fields, J. P. Zheng, R. S. Yang, and Z. L. Wang, "Intrinsic characteristics of semiconducting oxide nanobelt field-effect transistors," *Applied Physics Letters*, vol. 89, no. 9, Article ID 093114, 2006.

[39] C. Soci, A. Zhang, B. Xiang et al., "ZnO nanowire UV photodetectors with high internal gain," *Nano Letters*, vol. 7, no. 4, pp. 1003–1009, 2007.

[40] W. Kim and K. S. Chu, "ZnO nanowire field-effect transistor as a UV photodetector; optimization for maximum sensitivity," *Physica Status Solidi (A)*, vol. 206, no. 1, pp. 179–182, 2009.

[41] R. K. Joshi, Q. Hu, F. Am et al., "Au decorated zinc oxide nanowires for CO sensing," *Journal of Physical Chemistry C*, vol. 113, no. 314, pp. 16199–16202, 2009.

[42] Y.-S. Chiu, C.-T. Lee, L.-R. Lou et al., "Wide linear sensing sensors using ZnO:Ta extended-gate field-effect-transistors," *Sensors and Actuators B: Chemical*, vol. 188, no. 268, pp. 944–948, 2013.

[43] Y. Cui, "Nanowire nanosensors for highly sensitive and selective detection of biological and chemical species," *Science*, vol. 293, no. 5533, pp. 1289–1292.

[44] B. Huang, J.-C. Lin, and Y.-K. Yang, "ZnO/Silicon nanowire hybrids extended-gate field-effect transistors as pH sensors," *Journal of the Electrochemical Society*, vol. 160, no. 6, pp. B78–B82, 2013.

[45] H. H. Li, C. E. Yang, C. C. Kei et al., "Coaxial-structured ZnO/silicon nanowires extended-gate field-effect transistor as pH sensor," *Thin Solid Films*, vol. 529, no. 269, pp. 173–176, 2013.

[46] X. Liu, P. Lin, X. Q. Yan et al., "Enzyme-coated single ZnO nanowire FET biosensor for detection of uric acid," *Sensors and Actuators B: Chemical*, vol. 176, no. 316, pp. 22–27, 2013.

[47] A. Menzel, K. Subannajui, F. Güder, D. Moser, O. Paul, and M. Zacharias, "Multifunctional ZnO-nanowire-based sensor," *Advanced Functional Materials*, vol. 21, no. 22, pp. 4342–4348, 2011.

[48] A. Fulati, S. M. U. Ali, M. Riaz, G. Amin, O. Nur, and M. Willander, "Miniaturized pH sensors based on zinc oxide nanotubes/nanorods," *Sensors*, vol. 9, no. 11, pp. 8911–8923, 2009.

[49] R. S. Aga, D. Jowhar, A. Ueda et al., "Enhanced photoresponse in ZnO nanowires decorated with CdTe quantum dot," *Applied Physics Letters*, vol. 91, no. 23, Article ID 232108, 2007.

[50] S.-E. Ahn, H. J. Ji, K. Kim et al., "Origin of the slow photoresponse in an individual sol-gel synthesized ZnO nanowire," *Applied Physics Letters*, vol. 90, no. 15, Article ID 153106, 2007.

[51] H. Han, J. Kim, H. S. Shin, J. Y. Song, and W. Lee, "Air-bridged Ohmic contact on vertically aligned si nanowire arrays: application to molecule sensors," *Advanced Materials*, vol. 24, no. 17, pp. 2284–2288, 2012.

[52] J. H. He, C. H. Ho, and C. Y. Chen, "Polymer functionalized ZnO nanobelts as oxygen sensors with a significant response enhancement," *Nanotechnology*, vol. 20, no. 6, Article ID 065503, 2009.

[53] S. Koizumi, "Ultraviolet emission from a diamond pn junction," *Science*, vol. 292, no. 5523, pp. 1899–1901.

[54] C. S. Lao, M. Park, Q. Kuang et al., "Giant enhancement in UV response of ZnO nanobelts by polymer surface-functionalization," *Journal of the American Chemical Society*, vol. 129, no. 40, pp. 12096–12097, 2007.

[55] Y. Li, F. D. Valle, M. Simonnet, I. Yamada, and J. Delaunay, "Competitive surface effects of oxygen and water on UV photoresponse of ZnO nanowires," *Applied Physics Letters*, vol. 94, no. 2, 2009.

[56] L. Luo, Y. Zhang, S. S. Mao, and L. Lin, "Fabrication and characterization of ZnO nanowires based UV photodiodes," *Sensors and Actuators A: Physical*, vol. 127, no. 2, pp. 201–206, 2006.

[57] J. Zhou, P. Fei, Y. Gu et al., "Piezoelectric-potential-controlled polarity-reversible schottky diodes and switches of ZnO wires," *Nano Letters*, vol. 8, no. 11, pp. 3973–3977, 2008.

[58] R. Yan, D. Gargas, and P. Yang, "Nanowire photonics," *Nature Photonics*, vol. 3, no. 10, pp. 569–576, 2009.

[59] J. Zhou, Y. Gu, Y. Hu et al., "Gigantic enhancement in response and reset time of ZnO UV nanosensor by utilizing Schottky contact and surface functionalization," *Applied Physics Letters*, vol. 94, no. 19, Article ID 191103, 2009.

[60] Z. L. Wang, "Nanopiezotronics," *Advanced Materials*, vol. 19, no. 125, pp. 889–892, 2007.

[61] Y. Zhang, Y. Liu, and Z. L. Wang, "Fundamental theory of piezotronics," *Advanced Materials*, vol. 23, no. 27, pp. 3004–3013, 2011.

[62] Z. L. Wang, "Progress in piezotronics and piezo-phototronics," *Advanced Materials*, vol. 24, no. 34, pp. 4632–4646, 2012.

[63] M. S. Arnold, P. Avouris, Z. W. Pan, and Z. L. Wang, "Field-effect transistors based on single semiconducting oxide nanobelts," *The Journal of Physical Chemistry B*, vol. 107, no. 3, pp. 659–663, 2003.

[64] H. R. Byon and H. C. Choi, "Network single-walled carbon nanotube-field effect transistors (SWNT-FETs) with increased Schottky contact area for highly sensitive biosensor applications," *Journal of the American Chemical Society*, vol. 128, no. 7, pp. 2188–2189, 2006.

[65] S. N. Das, K. Moon, J. P. Kar et al., "ZnO single nanowire-based UV detectors," *Applied Physics Letters*, vol. 97, no. 2, 2010.

[66] L. Dong, S. Niu, C. Pan, R. Yu, Y. Zhang, and Z. L. Wang, "Piezo-phototronic effect of CdSe nanowires," *Advanced Materials*, vol. 24, no. 40, pp. 5470–5475, 2012.

[67] G. Cheng, X. Wu, B. Liu, B. Li, X. Zhang, and Z. Du, "ZnO nanowire Schottky barrier ultraviolet photodetector with high sensitivity and fast recovery speed," *Applied Physics Letters*, vol. 99, no. 20, 2011.

[68] F. Zhang, Y. Ding, Y. Zhang, X. Zhang, and Z. L. Wang, "Piezo-phototronic effect enhanced visible and ultraviolet photodetection using a ZnO-CdS core-shell micro/nanowire," *ACS Nano*, vol. 6, no. 10, pp. 9229–9236, 2012.

[69] S. Lu, J. J. Qi, S. Liu et al., "Piezotronic interface engineering on ZnO/Au-based schottky junction for enhanced photoresponse of a flexible self-powered UV detector," *ACS Applied Materials & Interfaces*, vol. 6, no. 16, pp. 14116–14122, 2014.

[70] T. Y. Wei, P. H. Yeh, S. Y. Lu, and Z. L. Wang, "Gigantic enhancement in sensitivity using Schottky contacted nanowire nanosensor," *Journal of the American Chemical Society*, vol. 131, no. 48, pp. 17690–17695, 2009.

[71] R. W. Scott, S. M. Yang, G. Chabanis, N. Coombs, D. E. Williams, and G. A. Ozin, "Tin dioxide opals and inverted opals: near-ideal microstructures for gas sensors," *Advanced Materials*, vol. 13, no. 19, pp. 1468–1472, 2001.

[72] B. Wang, L. F. Zhu, Y. H. Yang, N. Xu, and G. Yang, "Fabrication of a SnO_2 nanowire gas sensor and sensor performance for hydrogen," *Journal of Physical Chemistry C*, vol. 112, no. 17, pp. 6643–6647, 2008.

[73] J. Herrán, I. Fernández, R. Tena-Zaera, E. Ochoteco, G. Cabañero, and H. Grande, "Schottky diodes based on electrodeposited ZnO nanorod arrays for humidity sensing at room temperature," *Sensors and Actuators B: Chemical*, vol. 174, no. 319, pp. 274–278, 2012.

[74] S. Niu, Y. Hu, X. Wen et al., "Enhanced performance of flexible ZnO nanowire based room-temperature oxygen sensors by piezotronic effect," *Advanced Materials*, vol. 25, no. 27, pp. 3701–3706, 2013.

[75] C. Y. Lu, S. P. Chang, S. J. Chang et al., "ZnO nanowire-based oxygen gas sensor," *IEEE Sensors Journal*, vol. 9, no. 4, pp. 485–489, 2009.

[76] Z. L. Wang, "Piezopotential gated nanowire devices: piezotronics and piezo-phototronics," *Nano Today*, vol. 5, no. 6, pp. 540–552, 2010.

[77] L. Wu, F. Song, X. Fang, Z. Guo, and S. Liang, "A practical vacuum sensor based on a ZnO nanowire array," *Nanotechnology*, vol. 21, no. 47, Article ID 475502, 2010.

[78] G. Hu, R. Zhou, R. Yu, L. Dong, C. Pan, and Z. L. Wang, "Piezotronic effect enhanced Schottky-contact ZnO micro/nanowire humidity sensors," *Nano Research*, vol. 7, no. 7, pp. 1083–1091, 2014.

[79] P. H. Yeh, Z. Li, and Z. L. Wang, "Schottky-gated probe-free ZnO nanowire biosensor," *Advanced Materials*, vol. 21, no. 48, pp. 4975–4978, 2009.

[80] Y. Liu, Z. Y. Zhang, Y. F. Hu, C. H. Jin, and L. Peng, "Quantitative fitting of nonlinear current-voltage curves and parameter retrieval of semiconducting nanowire, nanotube and nanoribbon devices," *Journal of Nanoscience and Nanotechnology*, vol. 8, no. 1, pp. 252–258, 2008.

[81] R. Yang, Y. Qin, L. Dai, and Z. L. Wang, "Power generation with laterally packaged piezoelectric fine wires," *Nature Nanotechnology*, vol. 4, no. 1, pp. 34–39, 2008.

[82] S. Mao, G. Lu, K. Yu, Z. Bo, and J. Chen, "Specific protein detection using thermally reduced graphene oxide sheet decorated with gold nanoparticle-antibody conjugates," *Advanced Materials*, vol. 22, no. 32, pp. 3521–3526, 2010.

[83] C. Pan, Z. Li, W. Guo, J. Zhu, and Z. L. Wang, "Fiber-based hybrid nanogenerators for/as self-powered systems in biological liquid," *Angewandte Chemie International Edition*, vol. 50, no. 47, pp. 11192–11196, 2011.

[84] R. Yu, L. Dong, C. Pan et al., "Piezotronic effect on the transport properties of GaN nanobelts for active flexible electronics," *Advanced Materials*, vol. 24, no. 26, pp. 3532–3537, 2012.